We are IntechOpen, the world's leading publisher of Open Access books Built by scientists, for scientists

4,800
Open access books available

122,000
International authors and editors

135M
Downloads

Our authors are among the

154
Countries delivered to

TOP 1%
most cited scientists

12.2%
Contributors from top 500 universities

CLARIVATE ANALYTICS BOOK CITATION INDEX INDEXED

WEB OF SCIENCE™

Selection of our books indexed in the Book Citation Index in Web of Science™ Core Collection (BKCI)

Interested in publishing with us?
Contact book.department@intechopen.com

Numbers displayed above are based on latest data collected.
For more information visit www.intechopen.com

5

Fabrication and Applications of Metal Nanowire Arrays Electrodeposited in Ordered Porous Templates

Giray Kartopu[1] and Orhan Yalçın[2]
[1]*University of Nottingham, Nottingham NG7 2RD,*
[2]*Niğde University, 51240 Niğde,*
[1]*UK*
[2]*Turkey*

1. Introduction

At present, there is a huge anticipation that the realm of nanotechnology will soon be realized, and the life will become easier and more enjoyable – thanks to numerous new products and apparatus that will be operating on 'nano-facts' and nano-sized objects. Material properties and functionalities of the bulk tend to differ when one or more of its dimensions are reduced down to between 100 to 1 nm, the so called 'nanosize regime'. Thin films (two dimensional, or 2D), nanowires/nanotubes (one dimensional, or 1D), and nanoparticles/quantum dots (zero dimensional, or 0D) constitute the basic classes of nanomaterials. Among these, particularly the 1D-materials are highly desirable, as their geometric shape and high surface area impart high functionally. For example, metal nanowires (MNWs) are likely to become an integral part of future nanodevices, at least as the elements interconnecting the functional components such as 'nano'-transistors.

Additional to the provision of electrical connection to nano-circuits, the MNWs are expected to be utilized as the functional components in various applications ranging from high density perpendicular data storage to nano-sensors, from high-sensitivity nano-electrodes to meta-materials, and so on. In this chapter, we shall focus on the potential applications of MNWs that are synthesized via the template fabrication method.

Template synthesis of MNWs arrays comprises the electrochemical reduction of the ions of one/more desirable metals inside the nano-pore channels of an insulating membrane fabricated via self-assembly. Owing to its cost effectiveness, versatility and high throughput the template fabrication, being a bottom up synthesis method, offers significant promise for the production of versatile, tailor-made MNWs.

For most end applications, it is desirable to have MNWs with high aspect ratio (ratio of wire length to diameter) and/or specific surface area, production reproducibility as well as uniformity in wire size and shape in conjunction with high spatial ordering. Thus, the self-organized porous anodic aluminium oxide (AAO) membrane, displaying most of the desirable template properties, has become the centre of focus for MNWs synthesis.

Source: Electrodeposited Nanowires and Their Applications, Book edited by: Nicoleta Lupu,
ISBN 978-953-7619-88-6, pp. 228, February 2010, INTECH, Croatia, downloaded from SCIYO.COM

In what follows we shall first examine the fabrication and properties of the AAO template. Next, the electrochemical template synthesis of both single-component and multilayered/ superlattice MNWs will be described. Finally, major applications of these MNWs will be presented.

2. Preparation and properties of anodic aluminum oxide templates

2.1 History and background

Formation of porous as well as barrier-like alumina films by aluminium anodization is a well known procedure which has been studied since 1950s [Keller et al., 1953]. Today it has found its way to aviation industry [Avcorp Inc., 2009], and even to our everyday life, e.g. through kitchen utensils, where an industrial scale hard-anodization is performed to give the aluminium a protective finish rendering it thermally and mechanically resistant and non sticky.

Anodization of aluminium usually takes place in a suitable acidic solution comprising of chromic/phosphoric/sulphuric/oxalic/malonic acid in water at a fixed current density (galvanostatic) or, more commonly, at a fixed bias (potentiostatic). In the case of porous films, the pore and cell dimensions as well as pore regularity are strong functions of the applied potential. For example, the established growth rate for the cell size, or the pore (center-to-center) distance, is 2.5 nm/V [O'Sullivan & Wood, 1970]. Steady-state porous film formation is maintained by the equilibrium between Al oxidation and oxide-dissolution at the pore base. Since oxygen is incorporated in the anodic film (in the form of Al_2O_3), the volume (thickness) of the formed film is higher than that of the consumed Al. Optimal conditions for the self assembly of highly ordered pore arrangements were discovered only after 1995 [Masuda & Fukuda, 1995; Li et al., 1998]. Today, such ordered porous films are widely employed as mass fabrication tools, i.e. 'templates', for a myriad of 1D and composite nanomaterials in the name of fundamental and/or technological interests [Martin, (1994); Wade & Wegrowe, (2005)]. The template synthetic method is so versatile [Hurst et al., 2006; Das, B. & Singaraju, P. (2005); Liang et al., (2002)] that its applications are as vast as the imagination!

2.2 Ordered porous aluminum oxide films by double-anodization

Pore formation in aluminium oxide films initiates at random locations on the aluminium surface, and as the anodization progress a self organisation process takes place, which dictates termination/merging of 'bad' pores, resulting in an ordered 2D hexagonal arrangement (Fig. 1a). This principle forms the basis idea in the formation of highly ordered AAO templates via the 'double-anodization' method [Masuda & Fukuda, 1995]. In this method, the initially formed porous oxide film, with rather less organised top layers, is removed and the anodization is repeated under similar conditions. As the pores reaching at the aluminium surface have tube-end-like shapes, removal of the first oxide film leaves the aluminium surface with highly ordered semi-spherical etch pits (Figs. 1b, 2a), which thereupon act as seeds for the ordered pore formation via the second anodization, resulting in non-intersecting, uniform pore channels running straight through the AAO film (Figs. 1c, 2b).

For template synthesis applications, double-anodized AAO templates are highly preferable over single-anodized or commercially available AAO membranes (e.g. Whatman Anodisc™ filters) as the latter lacks uniformity in pore size and shape and has little or no long-range

pore ordering. Further, often the quoted (nominal) average pore size in commercial specimens shows strong deviations throughout the film.

(a) (b) (c)

Fig. 1. Schematic representation of ordered AAO formation via double-anodization: (a) first anodization, (b) removal of the first (disordered) oxide, and (c) second anodization.

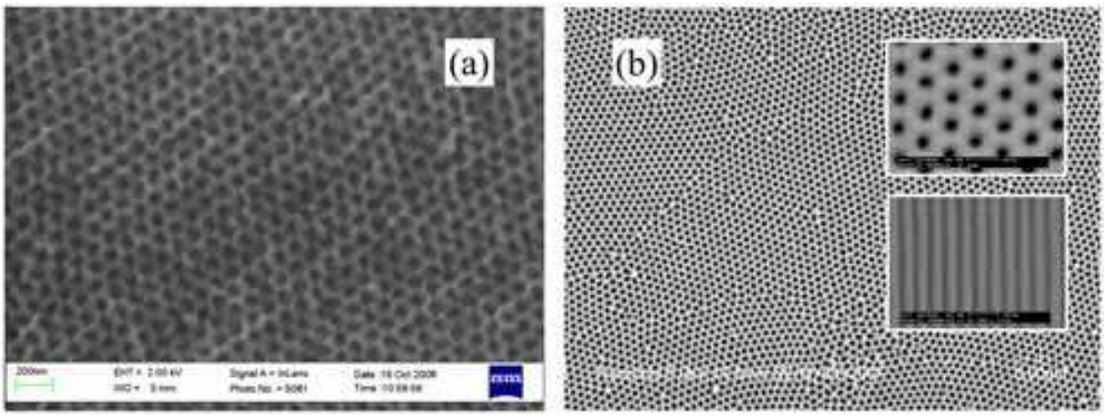

Fig. 2. SEM image of (a) the Al surface upon removal of the first anodic oxide film, and (b) the second anodic oxide film (insets: close-up view of the pore channels). Anodization was performed in 0.3M oxalic acid, at 40V and 15 °C (24h first anodization).

Commercial templates are typically prepared and lifted off from the supporting aluminium substrate using a single anodization procedure employing a step-wise voltage reduction method [Furneaux & Rigby, 1989]. In this process, the anodization voltage is gradually reduced near the end to about 0V, causing pore splitting, i.e. by formation of cracks in the alumina 'barrier layer' at the pore bottoms, followed by the detachment of the entire AAO film (owing to its diminished bonding to the Al substrate). Consequently, pores are much smaller and disordered at membrane surfaces compared to the film interior, albeit it is typically the surface porosity that is quoted in product descriptions as these membranes are usually produced for filtration applications. Figs. 3a and 3b compares tilted cross-sections of an AAO Anodisc™ membrane having nominal pore size of 200 nm with an AAO film double-anodized in 0.3M oxalic acid at 40V (to enhance imaging pores in AAO film were enlarged using an isotropic chemical etching following the second anodization). The contrast in the pore uniformity between these templates is further highlighted in Figs. 3c and 3d where mechanical polishing is applied subsequent to metal-pore filling by electroplating (see Section 3 for details on electrochemical template synthesis).

Detailed structural characterizations performed by transmission electron microscopy (TEM) analysis on AAO films anodized under different conditions reveal that porous alumina necessitates a porosity of about 10% to be self ordered [Nielsch et al., 2002]. There are three well-established anodizing regimes that yield in AAO films of this type (Table 1) [Li et al., 1998]. As the pH of solution is lowered the dissolution rate at the pore base increases, and

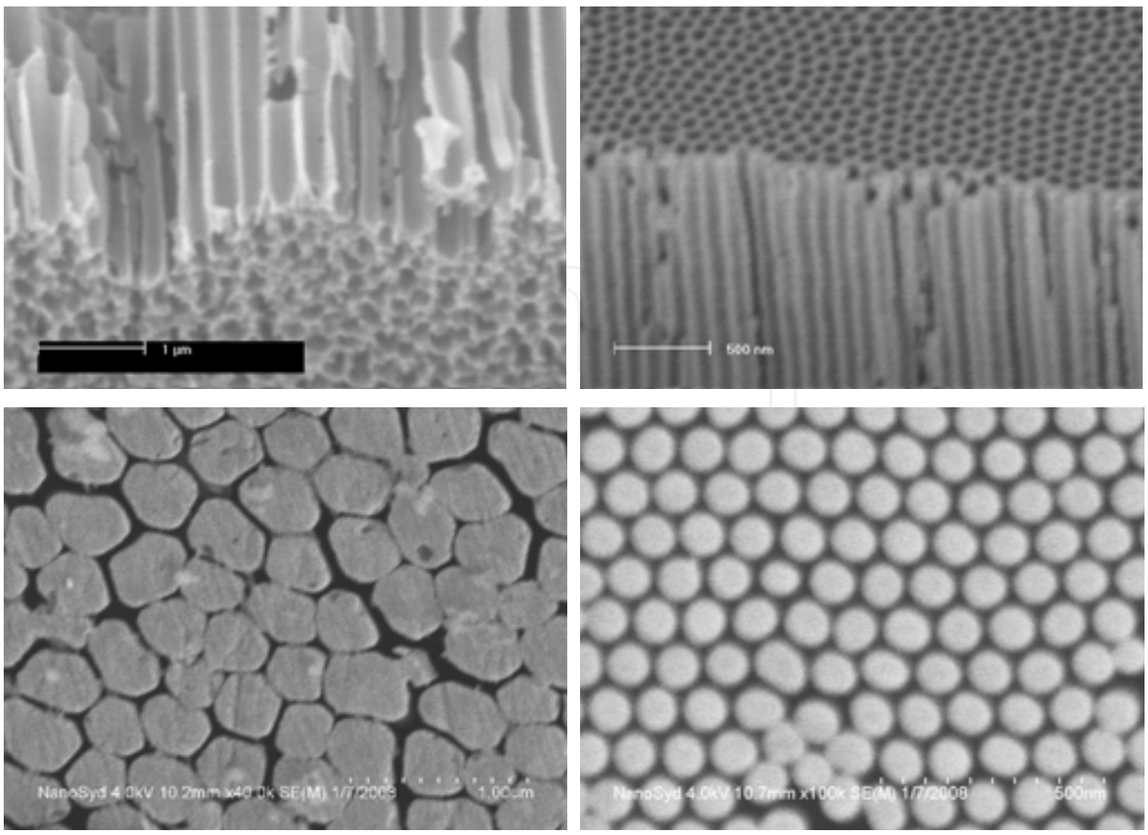

Fig. 3. Cross sectional view of (a) Anodisc™ AAO (quoted pore size 200 nm) and (b) doubleanodized AAO (0.3M oxalic acid, 40V). (c, d) Topographic view of the same templates upon pore filling and subsequent mechanical polishing (bright features correspond to metal nanowires; dark regions correspond to AAO pore walls).

Electrolyte	Bias (V)	Interpore distance (nm)	Pore density (per cm^2)
H_2SO_4 (sulphuric acid)	25	63	~10^{11}
$C_2H_2O_4$ (oxalic acid)	40	105	~10^{10}
H_3PO_4 (phosphoric acid)	195	500	~10^9

Table 1. The three well-established anodization conditions that lead to self-ordered porous AAO films.

thus, lower potentials are favored for the self-sustainable growth of ordered AAO films. Therefore, different self ordering voltages exist for different acid types. As pointed out earlier, the interpore distance, or the cell size, (L) is defined by the applied potential with a proportionally constant of 2.5 nm/V [O'Sullivan & Wood, 1970]. In accord, commonly observed values for self ordered AAO films, if obtained in the above regimes, are L ≈ 63, 105 and 500 nm, respectively (Table 1). Outside the optimal range of the anodization potential the porosity can be remarkably different. For example, reducing the potential from 195 to 160 V in phosphoric acid increases the film porosity to about 40% [Nielsch et al., 2002]. Increasing the potential from 40 to 120-150V in oxalic acid (under extreme cooling of the Al/electrolyte

interface) decreases the porosity to about 3% [Lee et al., 2006]. The electrolyte temperature and concentration, on the other hand, have only minor effects on template parameters and are usually set to 0-20 °C and 0.1-0.4 M, respectively. For example, increasing the concentration of sulphuric acid from 1 to 10 wt %, i.e. from about 0.1 to 1 M, results in a mere 20% reduction in the cell parameter [Nielsch et al., 2002]. Volume expansion factor ($R = V_{Al2O3}/V_{Al}$) of ordered AAO having 10% porosity is determined to be about 1.2 [Jessensky et al., 1998].

In fact, additional to double-anodization strategy outlined above there are other factors used to improve the template parameters, e.g. the ordered pore domain size. Firstly, Al has to be annealed for 1-4 h in a non-oxidizing atmosphere, such as that of Ar or N_2, close to the melting temperature of Al (typically between 400-500 °C). Secondly, the Al surface has to be de-greased by an ultrasonic treatment in acetone, and then, electro-polished to a mirror finish in a perchloric acid/ethanol electrolyte, typically of 1:5 vol. ratio, at a bias of 15-25V for 15-60s (in this process, too, Al is connected as the anode). Finally, the initially non-circular pore channels can be rounded up, as well as intentionally widened, using post-anodization chemical etch, e.g. in dilute phosphoric acid at 30-35 °C for 5-15 min.

2.3 Highly ordered porous aluminum oxide films by aluminum pre-texturing

Size of the ordered pore domains in double-anodized AAO extends to a maximum of about 5 μm; large numbers of pore defects are still observed at the domain boundaries. In order to obtain ideally ordered films surface pre-texturing of aluminum has to be realized. Several methods have been tested for this purpose, and formation of even mono-domain AAO films has been demonstrated. As it can be predicted, despite its costliness and additional complexities, lithography aided Al pre-texturing does away the need to perform double/multiple anodizations since high pore ordering is readily obtained through a single anodization process. The following are the major routes taken to achieve ideal pore arrangements in anodic alumina:

- Imprint lithography (pattern transfer via embossing with a SiC mold [Masuda et al., 1997], SiN mold [Choi et al., 2003], commercial grating [Mikulskas et al., 2001], etc.),
- Focused ion-beam lithography (direct writing on Al [Peng et al., 2005; Robinson et al., 2007] or via photoresist patterning [Liu et al., 2003]),
- Interference/holographic lithography (laser interference [Sun & Kim, 2002; Krishnan & Thompson, 2007]),
- Pattern transfer via nano-sphere lithography (self assembly of colloidal particles followed by embossing [Fournier-Bidoz et al., 2004] or reactive-ion etching [Kim et al., 2007]), and
- Pattern transfer via (Al) deposition on nano-structured substrates [Nishio et al., 2008].

Each of these approaches has its own advantages and disadvantages. For example, the molds, i.e. nano-patterned masters, used for embossing of Al have to be custom built for each application as they must contain nanoscale features that are compatible with the anodization conditions that lead to self assembly (see Table 1). Despite its cost efficiency and simplicity nano-sphere lithography cannot yield in mono-domains that extend over large scales since the self organisation of colloidal particles is inherently limited in perfection. Nevertheless, depending on the nature of the aimed end-product or the application, a particular method may stand out due to considerations related to the device geometry, functionality and/or financial issues. Fig. 4 presents two examples of ideally ordered AAO films obtained through Al pre-texturing.

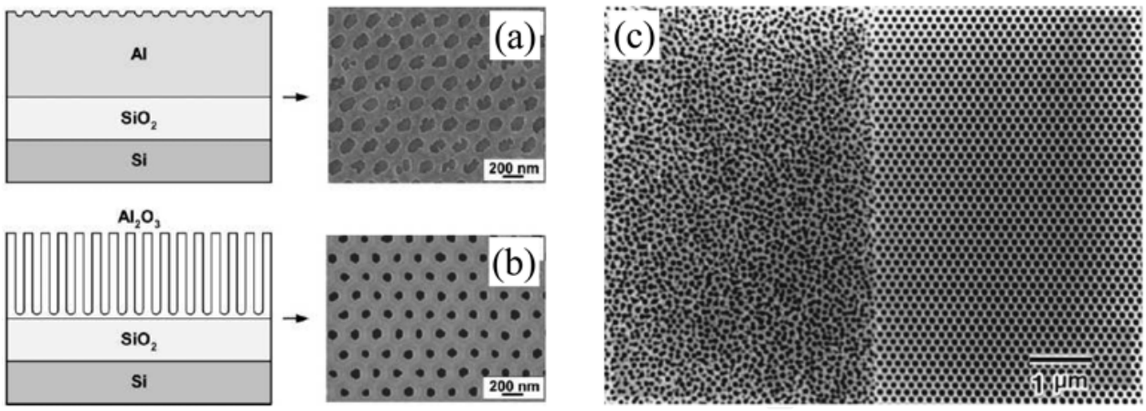

Fig. 4. Fabrication of ideally ordered porous alumina films using Al pre-texturing processes: Laser interference lithography (a, b) [Krishnan & Thompson, 2007. Copyright Wiley-VCH Verlag GmbH & Co. KGaA. Reproduced with permission.] and imprint lithography (c) (Reprinted with permission from [Masuda et al., 1997]. Copyright [1997], American Institute of Physics.). (a) Surface of an Al thin film (deposited on oxidized Si substrate) is patterned using interference lithography and wet-etching techniques, (b) pre-patterned Al film is anodized (at 86V in 5% H_3PO_4 solution), and (c) single-anodized (at 60V in 0.3M $C_2H_2O_4$ solution) Al foil surface without (left) and with (right) pre-texturing via imprint lithography.

3. Electrochemical synthesis of metal nanowires in anodic alumina templates

Electrochemical synthesis into anodic alumina pore channels can be realized once a conductive path is formed through the pore channels between the electrolyte (containing metal ions) and the deposition electrode at the bottom of the pores. This proves to be particularly difficult for anodic alumina films grown on Al foils as these films inherently have a thick (several tens of nm), insulating oxide (alumina) barrier layer that separates the pores from the Al metal.

3.1 Deposition into free-standing membranes

In order to circumvent the above problem there are two classical approaches one can follow. In the first case, first a sufficiently thick alumina film is formed on Al foil and then released to obtain a self-standing membrane with through pores using sequential chemical etching of the nonoxidized Al (Fig. 5a) and the alumina barrier layer (Fig. 5b). Physical vapour deposition of a thin metal film on one of the membrane surfaces (Fig. 5c) completes the process of obtaining the desired sample geometry to begin electro-deposition process. (This is also the geometry attained when using other free-standing membranes, such as commercial polycarbonate filters [Schönenberger et al., 1997; Whitney et al, 2003], i.e. prior to electro-deposition). Electrodeposition of MNWs can then be performed using either two- or three-electrodes conventional direct-current (DC) plating (Fig. 5d). The MNWs grow from the bottom electrode in a bottom-up fashion. Thus, the length of wires can be controlled at will simply via changing the deposition time, or more correctly, the charge density. The process is governed by the Faraday equation, which takes into account the template parameters (pore size, pore density, porosity, etc.) as well as filling efficiency [Schonenberger et al., 1997].

(a) (b) (c) (d)

Fig. 5. Fabrication of MNWs via free-standing AAO membranes: a) dissolution of non-oxidized Al, b) removal of alumina barrier layer, c) metallization, and d) DC electroplating. Al can be selectively dissolved in an aqueous solution of $HgCl_2$, or $CuCl_2$:HCl, or $SnCl_4$ at the room temperature or under cooling. Barrier layer can be removed (and the pores rounded) by chemical etching in dilute (~5 wt. %) H_3PO_4 at 30-35 °C.

Using the free-standing AAO membranes, it is possible to substantially widen the pores by chemical etching, which in turn provides more flexibility in the tuning of nanowires' diameter and their associated physical properties. These membranes are resistant to heat treatments up to ~400 °C, after which they start to crystallize and, more importantly, become distorted via curling up. Furthermore, since it is difficult to obtain thick, self-standing AAO films with small pores this method is not suitable for the synthesis of MNWs having small diameters, i.e. <20 nm.

3.2 Deposition into on-substrate anodic alumina/Al templates

In the second case, the AAO layer is kept on the Al substrate while the barrier layer is thinned/cracked (Fig. 6a), using in-situ voltage reduction method and/or ex-situ (post-anodization) chemical etching, so as to facilitate its electrical conductivity. Nevertheless, as the barrier layer cannot be eliminated completely (to preserve the structural integrity of the AAO/Al pair), electrical conduction remains limited and hence it is necessary to use alternating-current (AC), rather than DC, deposition (Fig. 6b) employing a high voltage (~10-25V) and a high frequency (several hundred Hz) [Yin et al., 2001; Metzger et al., 2000].

(a) (b)

Fig. 6. Fabrication of MNWs via on-substrate AAO/Al template: a) barrier layer thinning, and b) AC electro-deposition.

As an advantage of this method, both thin and thick on-substrate AAO/Al templates can be used to prepare MNWs, thus permitting access to the sub-20 nm (pore/wire diameter) range. The process is relatively simpler compared to that utilizes free-standing membranes. However, the synthesized MNWs are often porous and polycrystalline, and are not well bonded to the Al electrode, which hinder the electrical characterization and electrical properties of the as-synthesized MNWs. Additionally, due to the existence of the thin 'in-between' alumina layer, it is not feasible to obtain self-standing MNW arrays on the (Al) substrate by the removal of the AAO template. Another disadvantage of this method is that the pores cannot be widened to relatively large values, as otherwise delamination of the

AAO film from the Al surface takes place [Nielsch et al., 2000]. Further, superlattice-type multilayer MNWs (see Section 3.4) cannot be prepared using the AC deposition method. The filling efficiency, i.e. percentage of filled pores, is largely dependent on the spatial uniformity of the method followed to thin down/crack the barrier layer. Finally, ex-situ heating experiments on the MNWs can be performed, in principle, only up to the melting temperature of Al (650 °C).

3.3 Deposition into supported thin film anodic alumina/metal/substrate templates

As for AAO films obtained through anodization of thin (~0.5-1 μm) Al films deposited on conductive or metal-coated substrates, often realized is the unique, bridge-like shape and thinness of the barrier layer [Crouse et al., 2005; Foong et al., 2009]. It is thus relatively easy to open the pore bottoms to the (conducting) substrate via a brief chemical etching (Fig. 7a). The MNWs can then be grown in the conventional bottom-up manner using DC electroplating (Fig. 7b).

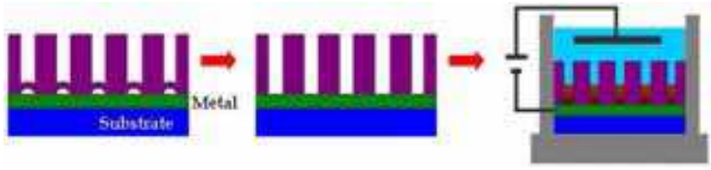

(a) (b)

Fig. 7. Fabrication of MNWs via supported AAO film: a) removal of bridge-like barrier layer, and b) DC electro-deposition.

Major benefits this method are that it allows ex-situ annealing temperatures up to 1000 °C [Mallet et al., 2005] and that robust free-standing MNW arrays can be obtained by etching of the thin film template [Matefi-Tempfli et al., 2009]. One of its drawbacks is that high vacuum deposition is required for the growth of Al films as well as several metallic interfacial layers, which typically entails an inert (Au or Pt) film (bottom electrode for electrodeposition) and a buffer layer(s), such as Ti, Nb, etc., used for adhesion and prevention of substrate oxidation via the anodization process. Moreover, the degree of pore ordering remains relatively poor, even if double-anodization is applied, because of the limited thickness of the starting Al film. Thus, for cases where pore/wire ordering is of crucial importance the Al pre-texturing method appears to be the most viable option.

3.4 Deposition of multilayer metal nanowires

Simple multilayered MNWs can be produced by changing the electrolyte and deposition bias for each component at a time. More complicated multilayer designs, such as the A/B/A/B/… type superlattice [Piraux et al., 1994], on the other hand, can be synthesized from a single bath by alternating the deposition voltage, albeit one of the layers always turning slightly impure (due to doping with other metals in the bath). In this process, the ionic concentration of the metal that can be reduced at lower (over)potentials is kept relatively very low (~1:100). At low potential pulse only these ions are deposited in layer A, whereas at higher potential pulse more than one type of ions is reduced in layer B. However, as there is a marked difference in ionic concentrations layer B is considered as nearly pure in the more concentric metal. Galvanostatic pulses can also be used to form multilayer MNWs. Fig. 8 illustrates close-up view of a Fe/Au (magnetic/optical) multilayer

nanowire obtained via galvanostatic pulses in an Anodisc™ AAO membrane with ~200 nm pores. Such MNWs combine useful properties of the respective components, offering enhanced functionalities with respect to those of the individual layers.

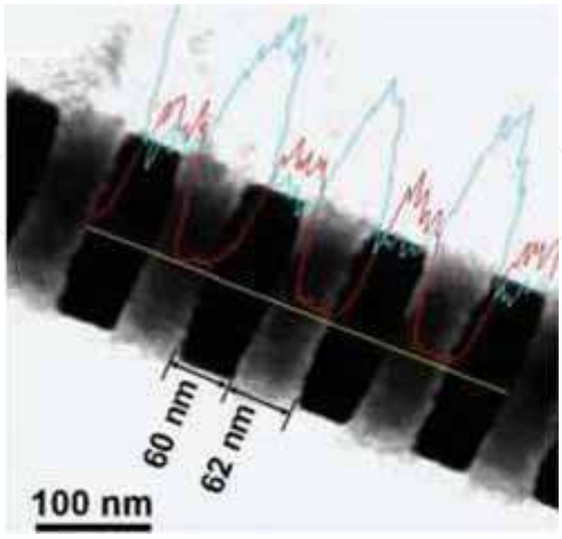

Fig. 8. Transmission electron micrograph and energy-dispersive X-ray elemental line scanning result (blue/light Fe, red/dark Au) of a superlattice nanowire obtained using 10 mA cm^{-2} (for Fe) and 0.5 mA cm^{-2} (for Au) pulses from an electrolyte containing $FeSO_4$, $KAu(CN)_2$, and H_3BO_3 with pH~3.5 [Lee et al., 2007. Copyright Wiley-VCH Verlag GmbH & Co. KGaA. Reproduced with permission.].

4. Applications of metal nanowires

4.1 Perpendicular magnetic data storage media

Recent roadmaps and reviews on hard disc drives indicate that a transition from longitudinal to perpendicular magnetic recording is taking place in these years, which may lead the storage density to increase to the 1 Tbit/in^2 levels [Kaitsu et al., 2006; Richter et al, 2007]. To realize perpendicular recording, it is necessary to have thin films containing high density of single-domain hard magnetic grains, or nano-particles, with out-of-plane anisotropy. In other words, magnetization easy axis of the individual recording elements (bits) must be aligned in the out-of-plane direction. Such anisotropy can be imposed, for example, by controlling either or both of the magneto-crystalline (via crystal orientation) and shape anisotropies of the magnetic particles. In this context, high aspect ratio nanoparticles or appropriately textured grains are desirable.

Due to the shape anisotropy effect, it is much easier to magnetize a 1D ferromagnet to its saturation using a longitudinal field. As depicted in Fig. 9a, for ferromagnetic nanowires below a critical diameter the single-domain state can be attained if the applied magnetic field is aligned parallel to the wire axis. On the other hand, multi-domain state results in if the field is applied in transverse direction (Fig. 9b). Compact nanowire arrays are, therefore, among the candidates for perpendicular storage applications. However, as for any magnetic system, the overall (effective) anisotropy of the nanowire array, and hence its suitability for these applications would be determined by many factors via the equation

$$H_{eff} = H_{shp} + H_{crys} + H_{elas} + H_x \quad (1)$$

where H_{eff} is the effective anisotropy field, H_{shp} the shape anisotropy field, H_{crys} the magnetocrystalline anisotropy field, H_{elas} the magneto-elastic (or strain related) anisotropy field, and H_x represents other fields present, e.g. the external field, magnetostatic (inter-particle) interaction fields, etc. Nanowire arrays embedded in ordered nano-templates thus represent a test-bed for the observation and investigation of these individual anisotropies.

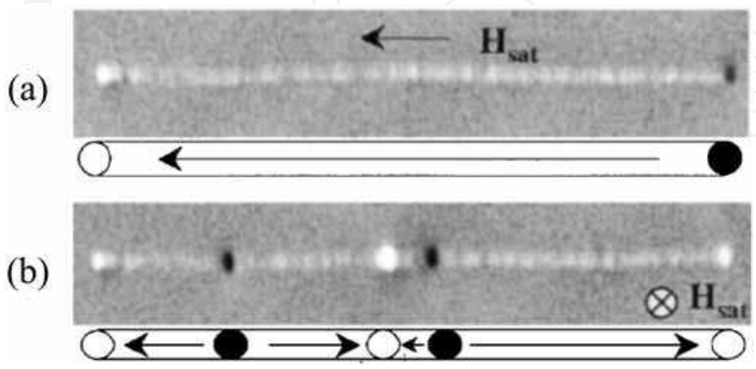

Fig. 9. Domain-imaging of a single 35 nm Co nanowire by magnetic force microscopy after saturation in a magnetic field applied (a) parallel and (b) perpendicular to wire axis (Reprinted with permission from [Ebels et al., 2000]. Copyright (2000) by the American Physical Society.). (For Co wires with aspect ratio of 10, the critical diameter is 140 nm.)

Ordered and high pore density AAO templates offer an opportunity to study the role of magnetostatic interactions [Clime et al., 2006; Fodor et al., 2008] as well as other anisotropies [Kumar et al., 2006] in determining the magnetic behaviour of densely packed ferromagnetic nanowire array films. Recently, size effects were investigated in uniform Co wires embedded in double-anodized oxalic acid AAO templates [Kartopu et al., 2008a]. Fig. 10 shows that the templates and arrays are well ordered. Magnetization data (Fig. 11) indicate that the axial hysteresis loops are sheared, that is quite large fields are required to saturate these arrays, due to strong magnetostatic (wire-wire) interactions. Effective anisotropy is determined by the interplay between the shape anisotropy and magnetostatic fields. As the wire diameter is increased magnetization easy-axis rotates from out-of-plane to in-plane direction. Further, as opposed to dipolar approximation, which suggests a continuous increase in interaction field with particle volume (length) [Grimsditch, 1998; Rivas et al., 2002], interestingly the H_{eff} or magnetostatic fields first tend to increase with wire length, i.e. the aspect ratio (τ) and then saturates. This behaviour is satisfactorily predicted by calculating the interaction energy for a pair of cylindrical ferromagnetic wires with high aspect ratio ($\tau > 2$) [Clime et al., 2006; Beleggia, 2004].

4.2 Giant-magnetoresistive multilayer nanowires

One of the early applications of template synthesized nanowires involved the use of magnetic/non-magnetic superlattice MNWs in realization of the giant magnetoresistance (GMR) effect in the current-perpendicular-to-plane (CPP) mode [Piraux et al., 1994]. The GMR effect, discovered in vacuum deposited (Fe/Cr) multilayer thin films by the late 1980s [Baibisch et al., 1988; Binasch et al., 1988] and commercialized in the late 1990s [Gochowski et al., 2003], has brought the 2007 Nobel Prize in Physics to its discoverers (Grünberg & Fert) [The Nobel Foundation, 2007]. High sensitivity of the GMR magnetic sensors ('readout

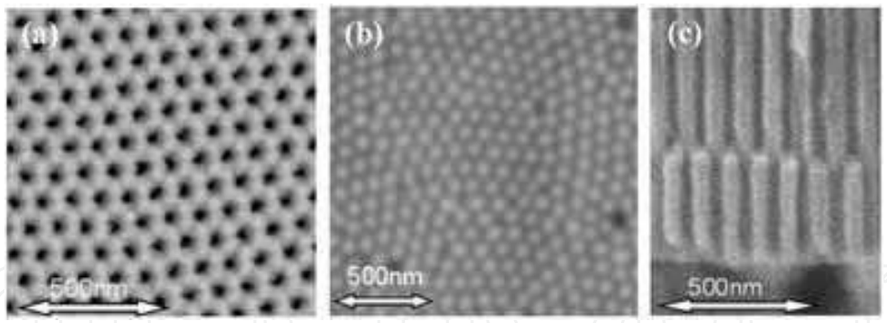

Fig. 10. Typical SEM image of (a) a double-anodized oxalic acid AAO film (~40 nm pore size), (b) topographic and (c) cross-sectional view of Co wire arrays deposited inside AAO pore channels (Reprinted with permission from [Kartopu et al., 2008a]. Copyright [2008], American Institute of Physics.).

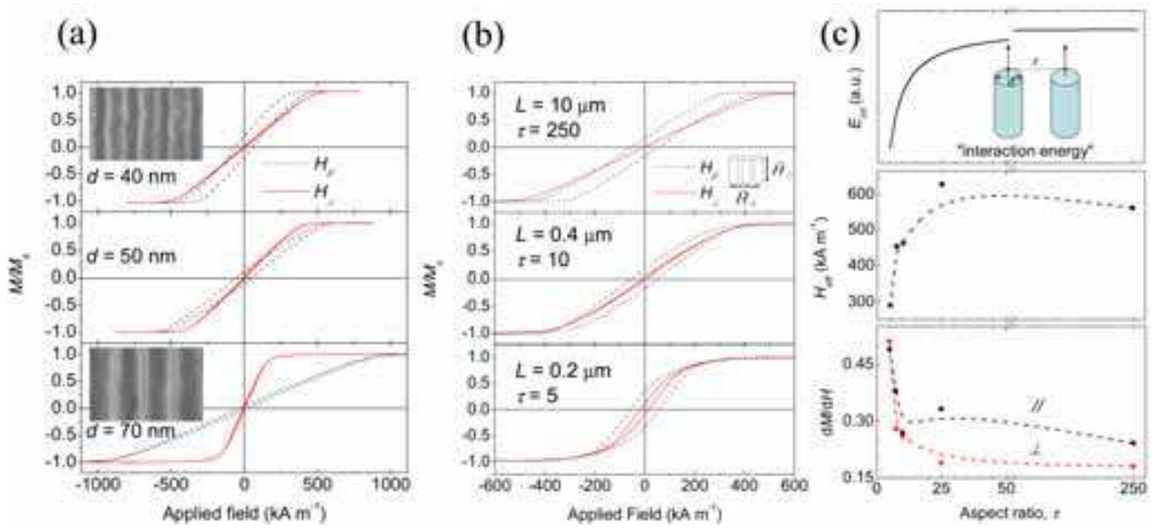

Fig. 11. Magnetization (M-H) curves as functions of (a) wire diameter (40-70 nm), and (b) wire length (0.2-10 μm) for Co nanowires in AAO templates collected parallel (dashed) and perpendicular (line) to wire axis. In (a) wire lengths are min. 4 μm; in (b), the wire diameter is fixed to about 40 nm. Insets in (a) show cross-sectional SEM images of the AAO templates used (dark lines correspond to pores). (c) Slope at zero field (dM/dH) and the effective anisotropy field (H_{eff}) calculated using the M-H curves in (b). Also shown (top panel) is the calculated magnetostatic interaction energy (E_{int}) for two axially magnetized intreracting wires with inverse distance of $\rho(r/d) = 0.4$ and $\tau > 2$ (Reprinted with permission from [Kartopu et al., 2008a]. Copyright [2008], American Institute of Physics.).

heads') enabled the enhancement of hard disc storage density. When the spins in the magnetic layers are aligned (e.g. upon application of an external field), resistance of the structure is reduced with respect to the initial 'random' spin state. In all-metal based thin film structures the GMR effect can practically be observed only when the flow of current is in the film plane (CIP mode) since the film resistances, and so the resulting GMR signal (fractional change in film resistance under applied field), are too low in the CPP configuration due to the insufficient film thickness (~1 μm). This is a drawback considered larger GMR values are expected in the CPP geometry [Pratt et al, 1991; Valet & Fert, 1993].

However, this is not the case for high aspect ratio MNWs in which the current naturally flows through the wire. Further, due to the fact that the relevant scaling lengths are the electron mean free path (λ_{mfp}) for the CIP geometry and the spin diffusion length (λ_{sdl}) for the CPP geometry and that $\lambda_{sdl} >> \lambda_{mfp}$ the 1D wire-like structure tolerates thicker layers. This, in turn, is beneficial to maintain a layer thickness uniformity and reproducibility from the production point of view.

Fig. 12 presents the first example of GMR-MNWs [Piraux et al., 1994]. The wires consisted of alternating Cu/Co layers pulsed deposited from a sulphate bath containing 10^{-3} M Cu ions and 0.5 M Co ions into the 10 μm long pore channels of a polycarbonate filter. At -0.2 V pulses almost exclusively Cu is deposited, while at -0.9 V pulses Co is deposited along with about 10% Cu. A thin Cu film evaporated onto the template surface ensured contacting of many wires to the bottom electrode (also Cu) deposited prior to electrodeposition process. Ferromagnetic characteristic of the Co layers was verified by magnetization measurements, and the maximum room temperature GMR measured about 15% (Fig. 12b).

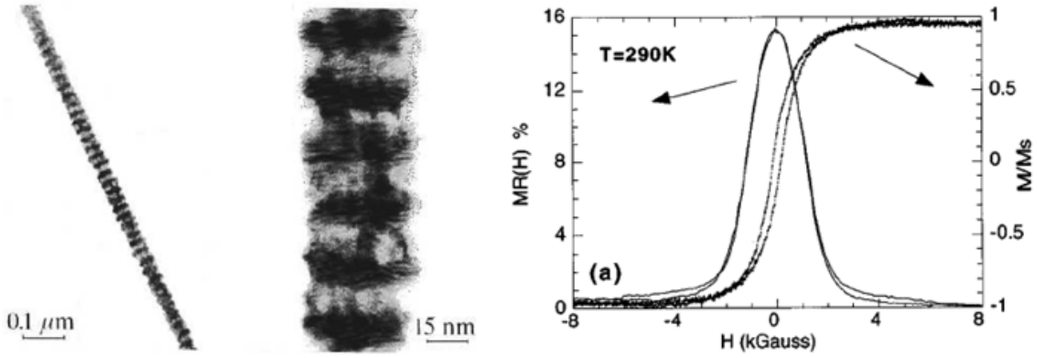

(a) (b) (c)

Fig. 12. (a, b) TEM images of [Co (10 nm)/Cu (10 nm)] multilayer nanowires (Co dark bands, Cu light bands), and (c) M-H curve and percentage magnetoresistance for a [Co (7 nm)/Cu (3 nm)]*1000 sample at room temperature (Reprinted with permission from [L. Piraux et al., 1994]. Copyright [1994], American Institute of Physics.).

In subsequent years, more studies on multilayer GMR-MNWs were conducted also utilizing Anodics™ [Evans et al., 2000; Tang et al., 2007] and double-anodized AAO [Ohgai et al., 2003; Tan et al., 2008; Huang et al., 2009] templates. It is claimed that the alumina template based nanowires provided larger values of GMR with respect to those grown in polycarbonate membranes [Evans et al., 2000; Ohgai et al., 2003]. Nevertheless, compared in general to the multilayer thin film systems the typical GMR values obtained from MNWs remain superior to those of electrodeposited thin films, and rather close to those of vacuum deposited thin films [Bakonyi & Peter., 2009]. Temperature dependent investigations on the effects of layers thickness and periodicity allowed the calculation of important physical values, such as λ_{sdl} and interface and bulk scattering parameters [Piraux et al., 1998], for the used metals. For example, λ_{sdl} of Co at room temperature is calculated to be ~38 nm, and a crossover from interface-dominated to bulk-dominated GMR occurs around Co layer thickness of 8 nm in Co/Cu multilayer MNWs. In another study, it is verified that the GMR of nanowires increased with the number of magnetic/non-magnetic bi-layers [Ohgai et al., 2003]. It is also observed that the nanowire arrays having isotropic properties, i.e. without definite easy axis of magnetization, display the highest magnetoresistance [Tan et al., 2008; Huang et al., 2009].

4.3 High resolution scanning probe microscopy tips

The spatial resolution of scanning probe microscopies depends heavily on the geometry and sharpness of the tip. Atomic force microscopy (AFM) enabled by carbon nanotube (CNT) tips is well known (see review article [Wilson & Macpherson, 2009]) and recently became commercialized [Nanosensors, 2008]. Metal based tips, on the other hand, are appealing for conducting AFM (also called electrical force microscopy, EFM), scanning surface potential microscopy (SSPM), and magnetic force microscopy (MFM) as well as AFM combined with near-field scanning optical microscopy (NSOM) or tip-enhanced Raman spectroscopy (TERS) [Renishaw plc, 2009; AIST-NT, 2009]. The CNT-tips can be obtained, for example, by chemical vapour deposition (CVD) from a catalyst particle at the end of a regular micro-fabricated AFM tip [Yenilmez et al., 2002], or by 'picking-up' from a substrate by scanning with a silicon tip [Hafner et al., 2001]. Metallic tips can be formed by electrochemical etching of a metal wire/tip [Gingery & Buhlmann, 2007], physically coating a CNT-tip [Deng et al., 2004], or by self assembly [Garcia-Martin et al., 2004]. Fig. 13 depicts an example of self assembly-prepared Co nanowire tip and its potential in MFM imaging.

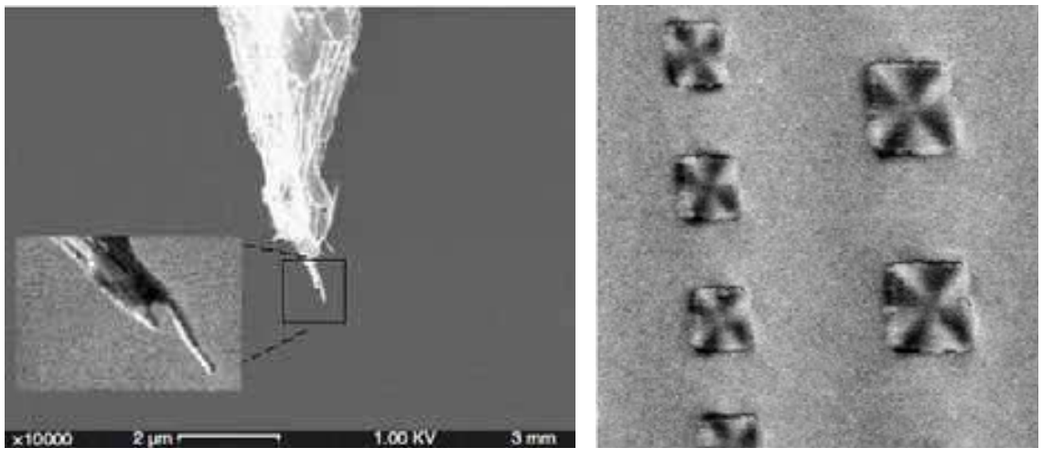

(a) (b)

Fig. 13. (a) A self-assembled 30 nm Co nanowire MFM tip, and (b) magnetic domains on NiFe micro-patterns (sides 400 and 600 nm) revealed using a tip as that in (a). Spatial resolution is about the wire diameter. [Garcia-Martin et al., 2004. IOP Publishing. Reproduced with permission.]

For a high aspect ratio Co wire the shape anisotropy field, $H_{shp} \approx 2\pi M_s$, amounts to 700 kA/m (~8800 Oe), where M_s is the saturation magnetization. Thus, even hard magnetic specimens can be studied using such nanowire-tips, without inflicting a change in the direction of tip's magnetic field, that is for sample (stray) fields of up to H_{shp}. Morever, it should be possible to improve the spatial resolution of the MFM imaging by further reducing the wire diameter.

4.4 Substrates for surface-enhanced Raman scattering

Surface-enhanced Raman scattering (SERS), a phenomenon known since 1970s [Fleischmann et al., 1974], relies on the electromagnetic enhancement (EM) on noble metal nanostructures for enhancing the Raman signal of surface-adsorbed chemical molecules. While ordinary

enhancements can be up to 10^6, in the late 1990s, even the Raman fingerprint of a single molecule was observed from certain nanoparticle aggregates, which also utilized other resonance effects [Nie & Emory, 1997]. In these experiments, Raman enhancements on the order of 10^{13}-10^{14} were calculated. There is a consensus now that the metal nanoparticles must be as close as possible, but not touching, to each other in order to provide such hot spots. Compact, ordered and controllable pore structure of porous AAO templates combined with the ease and versatility of metal nanowire/nanodot production by electrodeposition makes template fabricated metal nanostructures attractive for SERS studies. For these experiments, as illustrated in Fig. 14a, the templated metal nanostructures must be exposed to the electromagnetic excitation (typically a visible laser beam), which would also increase the area of metal surface for the adsorption of analyte molecules. Field enhancement for SERS in nanoparticle arrays has been studied by many researchers [Garcia-Vidal & Pendry, 1996; Kahl & Voges, 2000; Genov et al., 2004]. Particularly relevant here, the analytical result from [Genov et al., 2004] is plotted in Fig. 14b for an ordered vertically-aligned Ag nanowire array embedded in air at the wavelength of a common laser line (He-Ne, 633 nm):

$$G \cong \frac{\pi(m+1)^{7/2}}{2((4-\pi)m+4)\kappa^{7/2}} \times \sqrt{\frac{4t^2+9}{(t^2+1)^{3/2}} - \frac{t(4t^4+15t^2+15)}{(t^2+1)^3}} \tag{2}$$

where $m = |E_0|/E_1$, t = $(m/\gamma - 1)$, $E_m = E_0(1 - i\kappa)$ dielectric function of the metal, κ the loss factor, E_1 the dielectric function of the medium, and γ is the inverse interparticle distance (wire diameter/width of interparticle gap).

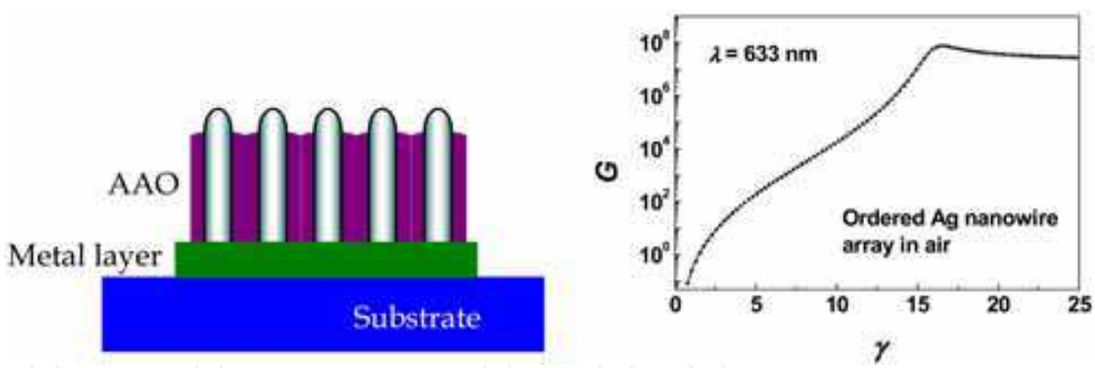

(a) (b)

Fig. 14. (a) Illustration of an array of MNWs partially exposed out of an AAO template, and (b) Calculated EM enhancement factor at 633 nm for an Ag nanowire array as in (a).

As can be seen from Fig. 14b, the EM enhancement factor (G) increases rapidly up to 10^8 with inverse distance (γ) and then saturates to a value about 10^7. With the addition of chemical (CHEM) enhancement (a factor of about 10^2 [Campion & Kambhampati, 1998]), arising mainly from the charge transfer between the molecule and substrate, typical SERS enhancement power of such a substrate can be as high as 10^{10}.

As a thumb of rule, the distribution in the length of electrodeposited nanowires in porous template channels increases with the wire length. Therefore, in order to have uniform length MNWs for SERS studies either the deposition time must be shortened, yielding nanodots rather than nanowires [Kartopu et al., 2006; Wang et al, 2006], or the initially long MNWs must be levelled by an appropriate post treatment, such as mechanical polishing [Kartopu et

al., 2008b] and ion milling [Sauer et al., 2005]. In the latter case, a chemical etching may be applied to increase the exposed area of nanowires (Fig. 15a and b). An in situ chemical etching (in dilute H_3PO_4) is used to probe the temporal change in the SERS spectrum of analyte molecules adsorbed on MNWs/Ag nanowires (Fig. 15c) [Sauer et al., 2005]. The signal intensity first increases to a maximum and then decreases rapidly before it completely vanishes. In the first regime, surface coverage of molecules increases with time, i.e. the area of newly-exposed (lateral) wire surfaces, while in the second regime the order of array coarsens considerably, and eventually leads to collapsing of the wires. The molecules attached to the lateral wire surfaces may experience stronger enhancements due to (increasing) interparticle interactions, i.e. multipolar fields. If this assumption is valid, it would also explain why a maximum is observed in Raman enhancement as well as the disappearance of the signal (when the wires start to make contact/collapse).

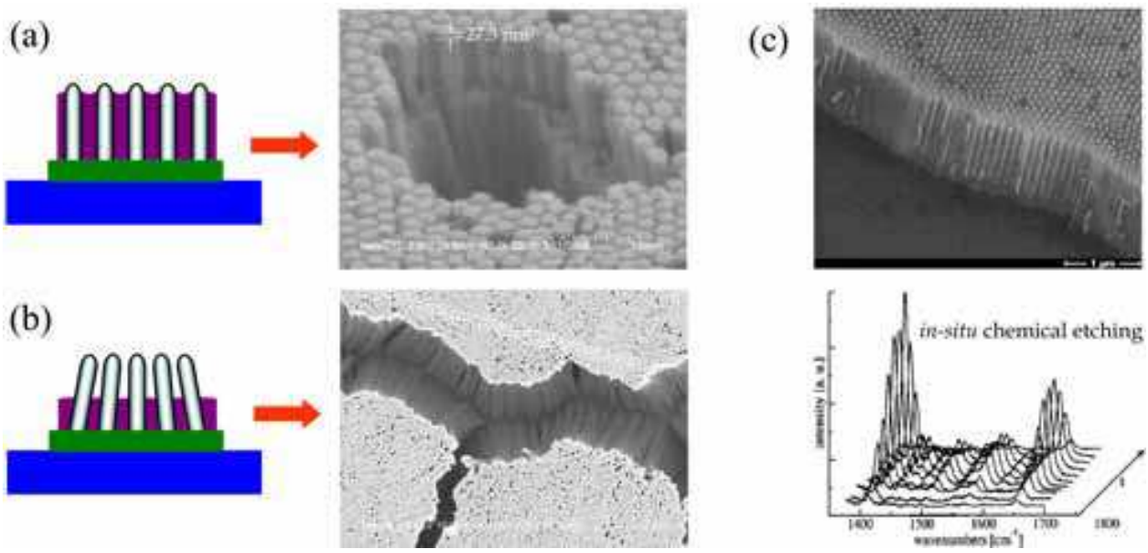

Fig. 15. Mechanically polished Ag nanowires/AAO composite after (a) 'mild-etching', and (b) 'over-etching' of the (AAO) pore walls in diluted H_3PO_4. (c) Data from [Sauer et al., 2005] (Reprinted with permission. Copyright [2005], American Institute of Physics.) showing (upper panel) a levelled Ag nanowire array in AAO and (lower panel) the dynamic change in the SERS spectrum of oxazine 170 molecules (adsorbed on Ag surfaces) excited at 633 nm with the in situ etching time. [A close-up view sample in (b) was also given as Fig. 3d].

4.5 Metamaterials

Another interesting use of MNWs fabricated in AAO templates could be in the field of negative index metamaterials, which are currently considered as the 'superlens' for high resolution imaging application. Metamaterials are artificially designed nano-composites possessing remarkable optical properties that do not exist in nature. They are capable of changing the propagation of light and can result in its negative refraction (Fig. 16a). Several theoretical models predict that metal-dielectric nano-composites based on a thin slab of AAO (dielectric) infiltrated with high aspect ratio Ag (or Au) nanowires can support a negative (effective) permittivity in the visible and infrared [Ao & He, 2005; Menon et al., 2008], meaning certain polarization of light could undergo negative refraction through this

medium. Experimental evidence on this phenomenon has recently been obtained (Fig. 16) [Yao et al., 2008].

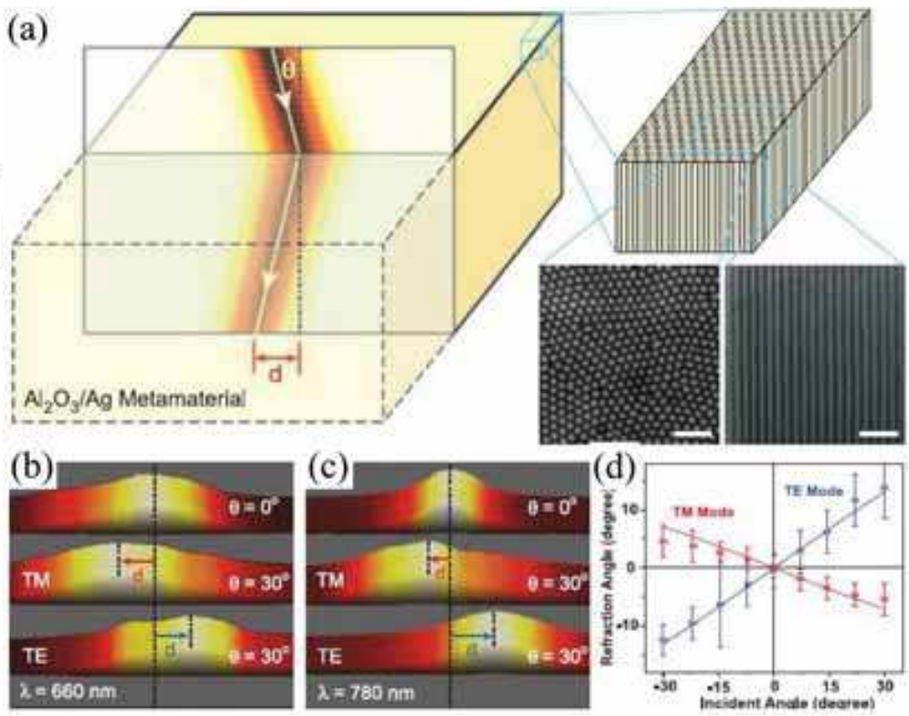

Fig. 16. The first experimental observation of negative refraction from the AAO/MNWs composite system. (a) Schematic of negative refraction through the Al_2O_3/Ag nanocomposite and close-up views of an ordered AAO template (scale bars: 500 nm). (b, c) Intensity and lateral displacement of the transmitted light (with respect to the centre of contact of the incident light) at two different wavelengths measured at the exit surface of AAO/Ag composite films of 4.5 μm (b) and 11 μm (c) thickness [horizontal size of (b) and (c) are 5 and 12 μm, respectively]. (d) Dependence of refraction angles on incidence angle for TM and TE polarizations at 780 nm. The group refractive indices of the metamaterial are calculated to be -4.0 and 2.2 for TM and TE polarizations, respectively [Yao et al., 2008] (Copyright 2008 by the American Association for the Advancement of Science).

It is commonly reported that transmission/absorption spectra of Ag or Au nanowires synthesized in AAO pores display two distinct bands depending on the excitation conditions. One of these resonances occur near the position of bulk plasmon resonance characteristic of the metal (~380 nm for Ag and ~500 nm for Au) for both *S* (or TE) and *P* (or TM)-polarizations at all angles, while the other resonance band is observed in the red (for Ag nanowires) or infrared (for Au nanowires) wavelengths for only *P* (TM)-polarized light for incidence angles grater than about 10 degrees [Evans et al., 2008; Menon et al., 2008]. Consequently, while the former band is due to transverse resonance of the nanowires, the latter band occurring at higher wavelengths can be attributed to longitudinal plasmon resonances associated to the long axis of the nanowires. The longitudinal mode is shown by appropriate modelling to be a collective property of the nanowire array, rather than that of the individual wire, as otherwise it would be expected at much higher wavelengths (in

infrared) [Evans et al., 2008]. From these theoretical and experimental results it appears that the longitudinal resonance mode of nanowires has to be excited (with TM polarized light) for the AAO/MNWs composites to show the negative refraction phenomenon. Further studies should elicit further particulars of this interesting, low cost metamaterial system. Among potential application areas are waveguiding, imaging, optical communication, and biosensing [Yao et al., 2008; Kabashin et al., 2009].

4.6 Nano-optics and molecular electronics

Multi-layered or -segmented MNWs are expected to be used as novel characterization tools in fields of nano-optics and molecular electronics due to the fact that wire dimensions and composition can be precisely tuned and that the wires can be manipulated by simple solution-based processing methods [Martin & Baker, 2005; Hurst et al., 2006]. A recently developed technique, coined 'on-wire lithography (OWL)' [Qin et al., 2005], which results in notched nanowires with unprecedentedly small gaps is likely to provide huge impetus in these regards. In OWL, first an arbitrarily designed multi-layered MNW array is obtained in the pore channels of a nano-template as described in Sec. 3.4. The wires are then liberated by complete dissolution of the template and placed on a flat substrate. In order to prevent collapsing of the nanowire architecture in the final step, the top semi-surface of the wires is coated with a thin film that is resistant to chemical etching. Wires are then loosened off the substrate (by ultrasonic agitation), and then a selective chemical etch is applied to remove only certain metal segments. The result is notched, discontinuous nanowires with the backing of a thin film (Fig. 17).

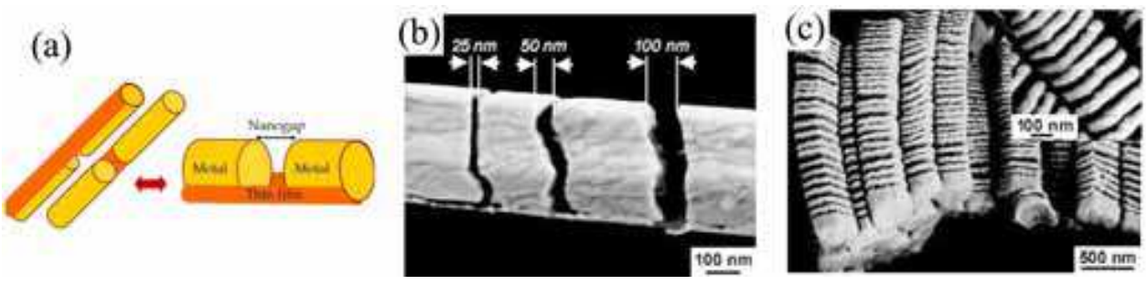

Fig. 17. OWL-produced notched nanowires: (a) Schematic illustration, and (b, c) micrographic views. Data reproduced from [Qin et al., 2005] (Copyrigt 2005 by the American Association for the Advancement of Science).

Nano-gaps down to 5 nm have been demonstrated, whereby dip-pen lithography-aided positioning of polymer molecules within 13 nm gapped-wires (contacted by standard microlithography techniques) provided evidence on the existence and electronic behavior, i.e. conductivity, of the molecules [Qin et al., 2005]. In another case, Au nano-discs with controlled sizes and gaps were obtained by OWL and employed in novel experiments designed for systematically studying hot spots produced due to interparticle couplings [Qin et al., 2006]. In these optical experiments, the electromagnetic enhancement (EM) was studied using SERS effect (see also Sec. 4.4), and it is verified that SERS enhancement factor was at least two orders of magnitude higher for any pairs/multiples of discs with a nanogap compared to an isolated disc. Further, optimum gap and disc sizes were determined at a given excitation wavelength. These experiments demonstrate the potential of multilayer MNWs in the fields of molecular electronics and nano-optics, considering that extremely

small nanogaps can be produced controllably and reproducibly using a simple method without the need of expensive lithography techniques.

4.7 Biological tags

Perhaps the most straightforward application of multi-segmented MNWs is in the field of biological labelling. Wires formed of metals that support strong plasmon resonances in the visible, i.e. Ag, Au, and Cu, can be routinely prepared having unique combinations of layer thicknesses and periodicities. These metals scatter visible light so strongly that even individual segments that are much smaller than the wavelength can be viewed using a standard optical microscope system with white illumination source (Fig. 18) [Nicewarner-Pena et al., 2001; Mock et al, 2002]. If spotted on a certain biomolecule, an arbitrarily-designed (or '-coded') multi-segment wire can act as a fingerprint for the rapid and simple identification of the biomolecule (among others). To exemplify the capabilities of this encoding system, a nanowire containing 13 segments and made of two metals (e.g. Ag/Au) is calculated to have 4160 permutations [Nicewarner-Pena et al., 2001].

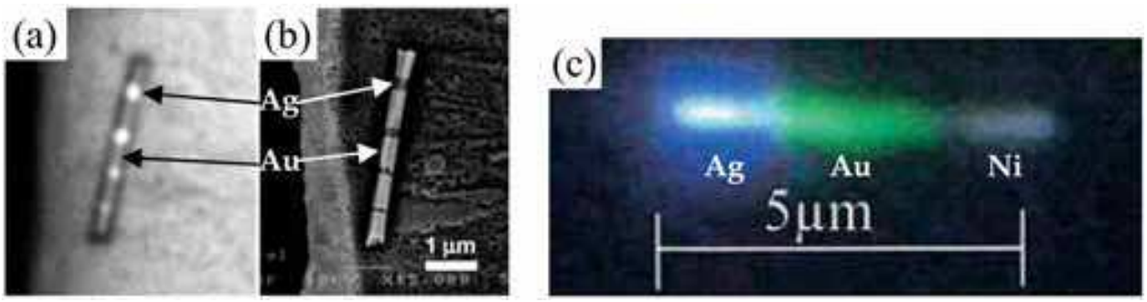

Fig. 18. (a) Optical and (b) SEM images of an Ag/Au multi-segmented nanowire with ~550 nm Au and 60, 110, 170, and 240 nm (bottom to top) Ag segments [Nicewarner- Peña et al., 2001] (Copyright 2001 by the American Association for the Advancement of Science). Ag segments look brighter in (a) and darker in (b). (c) Optical image of a three-metal nanowire (Reprinted with permission from [Mock et al, 2002]. Copyright [2002], American Chemical Society.).

4.8 Field-emission electron emitters

One-dimensional nanostructures (nanowire, nanotube) with high aspect ratio and low tip diameter are recognized as ideal field-emission (FE) electron sources, which are potentially useful as emitters in flat panel displays. Particularly carbon nanotubes (CNTs) have been the subject of considerable study [Heer et al., 1995; Collins & Zettl, 1997]. More recently, FE properties of 'nanowhiskers' of metal oxides [Luo et al., 2004] and metals [Kim et al., 2008] have also attracted interest. CNTs are usually produced by chemical vapour deposition (CVD) and hence requires high growth temperatures (>500 °C) which limits the choice of substrate. In addition, nanowiskers lack structural alignment and makes it difficult to control the density and aspect ratio of the emitters which are important parameters for tuning the FE threshold and current density. Therefore, use of template-synthesized CNTs [Quy et al., 2006] and room-temperature electodeposited MNWs [Vila et al., 2004] in ordered templates becomes attractive for FE applications. Fig. 19a depicts the common triode-type

experimental set up for detecting nanotube/nanowire field emission. Typically a high voltage on the order of a few kV is applied to the cathode (sample) for it to emit brightly. The current-voltage (I-V) characteristics are usually analysed with the Fowler-Nordheim (F-N) relationship:

$$J = A\left(\frac{\beta^2 E^2}{\phi}\right)\exp\left(-\frac{B\phi^{3/2}}{\beta E}\right) \tag{3}$$

where A and B are constants, β is the field enhancement factor, ϕ work function of the metal, and the electric field is given by $E = V/d$ with V the applied voltage and d the grid-cathode distance (spacer thickness, see Fig. 19a). The enhanced local field at the wire/tube tip is given by $E_t = \beta E$. Desirable properties for a FE device are the low turn-on voltage, high current density, and good emission homogeneity. Fig. 19b presents typical results for the grid and anode currents obtained from a Co nanowire array template-synthesized on a metallised silicon substrate [Vila et al., 2004]. In these experiments, the density of the wires was kept as low as $10^7/cm^2$ to avoid screening/interference effects between the wires [Collins & Zettl, 1997]. Ratio of anode to cathode currents is constant while the calculated enhancement factor was almost the same as the aspect ratio of the Co wires. The turn-on voltage (12 V/μm) is comparable to that of CNTs (1-10 V/μm) [Davydov et al., 1999]. Deviation from the F-N relationship (solid line) at higher fields is attributed to an undesired serial resistance (R = 4 MΩ) in the experimental set-up.

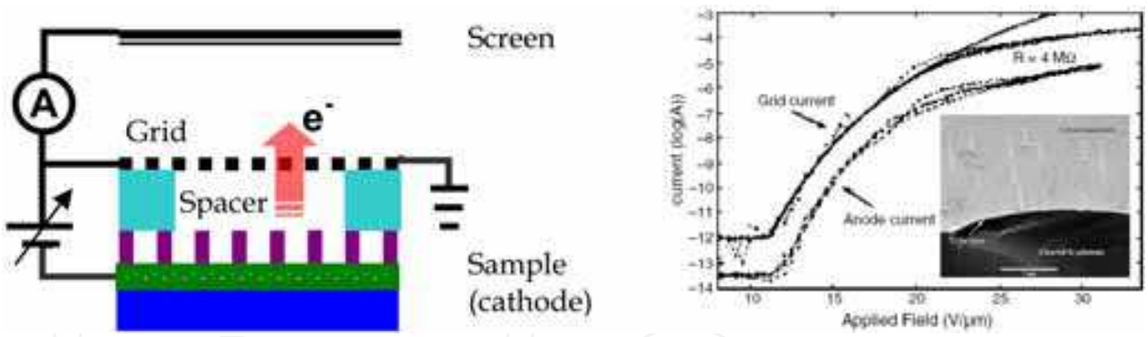

(a) (b)

Fig. 19. (a) Schematic of nanotube/nanowire FE experimental set-up (triode configuration). (b) FE characteristics of Co nanowires template-synthesized on metal-coated silicon substrate determined using a set-up similar to that in (a). Inset shows a micrograph of the Co nanowire array. (Data adapted from [Vila et al., 2004]. (Copyright [2004], American Chemical Society. Reproduced with permission.).

A unique advantage of field-emitting nanostructures' synthesis with thin film AAO templates (see also Sec. 3.3) is that established microelectronic processing technologies can also be applied to obtain FE display pixels and novel devices [Quy et al., 2006; Mátéfi-Tempfli et al., 2008]. Interest in recent theoretical studies focuses on optimum array parameters for maximum enhancement factor (β) and current density [Kim et al., 2009]. It is noted that β and current density, which are strong functions of the aspect ratio and spacing of emitters, applied field, and so on, actually do not require very dense arrays [Kim et al., 2009].

4.9 Gas sensors

Much of the work devoted to chemical sensors based on 1D nanostructures are aimed at developing high sensitivity gas sensors operating at low temperatures. Metal and metal oxide nanowires obtained on the step edges of highly-oriented pyrolytic graphite (HOPG) substrates have proven to be suitable for such sensing applications [Murray et al., 2004; Favier et al., 2001]. For example, palladium (Pd) nanowires were shown to exhibit excellent performance in the detection of high concentrations (above 2%) of hydrogen (H_2) [Favier et al., 2001]. This was explained to be due to the rather porous/discontinuous character of the Pd wires. When subjected to H_2 the Pd wires were observed, by *in situ* AFM imaging, to swell considerably (due to formation of PdH_x on Pd surfaces), thereby closing the gaps between nano-grains and allowing the wire to conduct electricity. Therefore, these peculiar wires acted effectively as hydrogen 'switches'. Despite the success of such HOGP-grown nanowires, other 'continuous' 1D architectures are desirable for sensing of low and ultra-low concentrations of H_2 and other gases (CO, NO_2, volatile organic compounds, etc.). With this aim in mind, several studies were conducted to synthesize and exploit MNWs in AAO templates [Kartopu et al., 2008c; Kim et al., 2006; Kolmakov et al., 2003]. Pd nanowires were DC electrodeposited in free-standing (Fig. 20a) as well as on-substrate thin film AAO templates (Fig. 20b). High sensitivity of such structures was verified using the set-up depicted in Fig. 20c, where the self-standing Pd array is contacted through the metallic substrate as the bottom contact and a sharp tip on the top. Fig. 20d shows that low concentrations (~0.2%) of H_2 can be detected in a reversible manner.

In another study, first metallic tin (Sn) nanowires were obtained by AC deposition in AAO templates, then released from the template and converted by thermal annealing to SnO_2 nanowires (30 nm radius), which were subsequently used in sensing experiments in the form of single-nanowire devices prepared by micro-contacting [Kolmakov et al., 2003]. It is observed that the initially conducting SnO_2 wire became dramatically an insulator in the presence of sufficient oxygen (ca. 10% in nitrogen), which indicates that charge-depletion (due to adsorption of oxidizing species in atmosphere) has deprived the entire wire of its carriers. The characteristic electron exchange length (Debye length, λ_D) for SnO_2 is on the order of ~40 nm (at 500 K). Accordingly, whilst charge-depletion remains to be a 'surface' phenomenon for the bulk, it was possible to switch low-diameter SnO_2 wires between the conducting and insulating states. Despite the promising results with phase-change MNWs, process of contact formation onto the sensing element (single wire or wire array) needs to be improved to increase sensitivity.

Recently, a simple yet effective approach has been introduced which yields metal-oxide-metal (MOM) nanowires (Fig. 21a) [Tresback et al., 2005]. In this process, first multi-segment MNWs are synthesized in AAO template, released from the template and then a segment of the wires is selectively oxidised by annealing at a temperature low enough to keep other segments metallic. Results pertaining to a single-wire (Au-NiO-Au) gas sensor (prepared by micro-contacting) are presented in Fig. 21b and c. Compared to an 'all-oxide' NiO single-wire device, the MOM sensor performs reasonably well for detecting low concentrations (<1%) of CO, despite the sensor response and recovery times are rather too long. Optimization would be needed for applications requiring compact sensors with low power consumption and high sensitivity. Such nanosensors, if combined in-parallel with others, are believed to lead to realization of the 'electronic nose' concept [Sysoev et al., 2006].

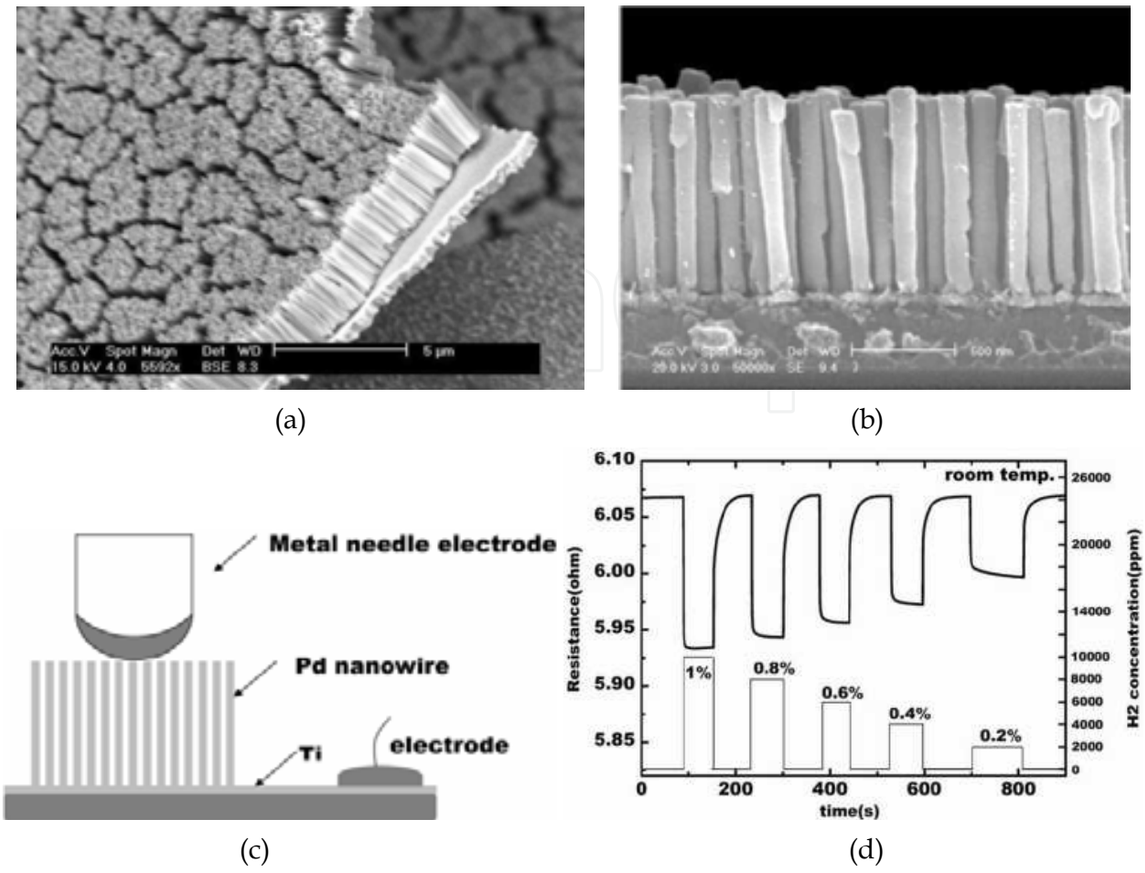

Fig. 20. Self-supporting Pd nanowires on metallic substrates prepared using free-standing (a) and supported thin film AAO (b) templates. (c) Set-up used for gas sensing experiments. (d) H_2-sensing performance of the array in (b) at room temperature. Data in (a) is reproduced with permission from [Kartopu et al., 2008c] (Copyright [2008], Elsevier). Data in (b-d) is reproduced with permission from [Kim et al., 2006] (© [2006], IEEE).

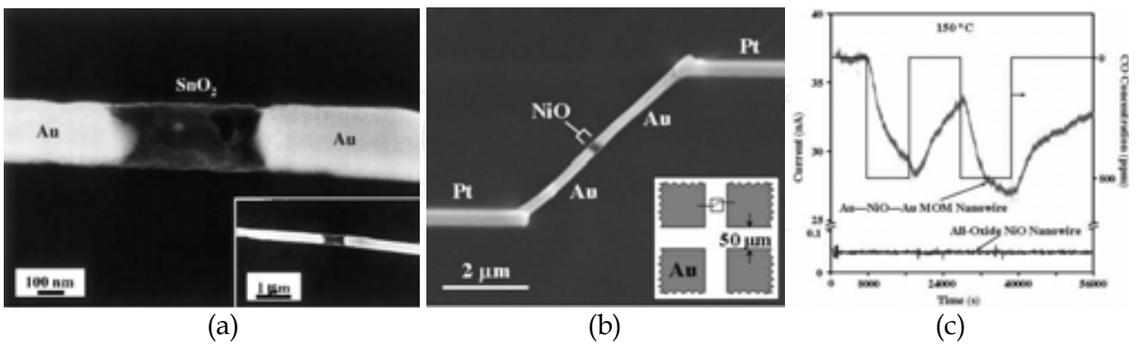

Fig. 21. (a) A template-synthesized Au-SnO_2-Au MOM nanowire at two different magnifications (Reproduced with permission from [Tresback et al., 2005] (© [2005], MRS). (b) Micrograph and (c) CO gas-sensing performance of a Au-NiO-Au MOM nanowire contacted using Pt-wires grown by focused ion beam (FIB) synthesis. In (c), also shown is the response of an all-oxide NiO nanowire synthesized and contacted in similar fashion (Reproduced with permission from [Tresback et al., 2008] (© [2008], MRS).

5. Conclusion

Fabrication, properties, and prominent applications of electrodeposited metal nanowires in porous anodic alumina templates have been presented. Both single component and multilayer nanowires can be prepared with ease, high reproducibility, and versatility. Compatibility of the produced structures with further processing methods, such as simple solution-based processing methods and established microelectronic processing technologies, makes these systems very attractive for a myriad of applications, ranging from chemical sensors to magnetic sensors, perpendicular data storage to field-emission electron sources, and from metamaterials to molecular electronics. Due to the limited spacing, and overlaps with previous reviews on the topic, several other interesting applications/properties, such as high-sensitivity nano-electrode arrays [Martin, 1994] and pH sensors [Antohe et al., 2009], superconductivity [Kline et al, 2006], thermoelectric power generation [Sommerlatte et al., 2007], etc. have not been presented. This chapter merely aimed at introduction of the basics and updated information on this young and dynamic research field, hoping that it will encourage both researchers and industry to make new initiations, and yield further nano-technological concepts and fruitful applications in various disciplines of science and engineering.

6. Acknowledgements

Financial support of TÜBİTAK (project 107T635) is gratefully acknowledged. One of the authors (GK) thanks to EU and Deutsche Forschung Gemeinschaft for several fellowships.

7. References

AIST-NT, (2009). Nanofinder R 30 - SmartSPM™ 1000: Confocal Raman / AFM combined system. http://www.aist-nt.com/wp-content/uploads/2009/04/reflection-ters-with- aist-afm.pdf

Antohe, V. A.; Radu, A.; Mátéfi-Tempfli, M.; Attout, A.; Yunus, S.; Bertrand, P.; Dutu, C. A.; Vlad, A.; Melinte, S.; Mátéfi-Tempfli, S. & Piraux, L. (2009). Nanowire-templated microelectrodes for high-sensitivity pH detection. *Appl. Phys. Lett*., 94, 073118-3.

Ao, X. & He, S. (2005). Negative refraction of left-handed behaviour in porous alumina with infiltrated silver at an optical wavelength. *Appl. Phys. Lett*., 87, 101112-3.

Avcorp Industries Inc., www.avcorp.com/section.asp?catid=152&subid=165&pageid=185, 2009.

Baibich, M.N.; Broto, J.M.; Fert, A.; Nguyen Van Dau, F.; Petroff, F.; Etienne, P.; Creuzet, G.; Friederich, A. & Chazelas, J. (1988). Giant magnetoresistance of (001)Fe/(001)Cr magnetic superlattices. *Phys. Rev. Lett.*, 61, 2472 – 2474.

Bakonyi, I. & Péter, L. (2009). Electrodeposited multilayer films with giant magnetoresistance (GMR): progress and problems. *Prog. Mater. Sci*., doi:10.1016/ j.pmatsci.2009.07.001.

Beleggia, M.; Tandon, S.; Zhu, Y. & De Graef, M. J. (2004). On the magnetostatic interactions between nanoparticles of arbitrary shape. J. Magn. Magn. Mater., 278(1-2), 270-284.

Binasch, G.; Grünberg, P.; Saurenbach, F. & Zinn, W. (1989). Enhanced magnetoresistance in layered magnetic structures with antiferromagnetic interlayer exchange. *Phys. Rev*. B, 39, 4828 – 4830.

Campion, A. & Kambhampati, P. (1998). Surface-enhanced Raman scattering. *Chem. Soc. Rev.*, 27, 241 - 250.

Choi, J.; Nielsch, K.; Reiche, M.; Wehrspohn, R.B. & Gösele, U. (2003). Fabrication of monodomain alumina pore arrays with an interpore distance smaller than the lattice constant of the imprint stamp. *J. Vac. Sci. Technol*. B, 21(2), 763-766.

Clime, L.; Ciureanu, P. & Yelon, A. (2006). Magnetostatic interactions in dense nanowire arrays. *J. Magn. Magn. Mater*., 297, 60-70.

Collins, P. G. & Zettl, A. (1997). Unique characteristics of cold cathode carbon-nanotube-matrix field emitters. *Phys. Rev. B*, 55(15), 9391 – 9399.

Crouse, M. M.; Miller, A. E.; Crouse, D. T. & Ikram, A. A. (2005). Nanoporous alumina template with in situ barrier oxide removal, synthesized from a multilayer thin film precursor. *J. Electrochem. Soc*., 152(10), D167 – D172.

Das, B. & Singaraju, P. (2005). Novel quantum wire infrared photodetectors. *Infrared Phys. Technol*., 46, 209 – 218.

Davydov, D. N.; Sattari, P. A.; AlMawlawi, D.; Osika, A.; Haslett, T. L. & Moskovits, M. (1999). Field emitters based on porous aluminium oxide templates. *J. Appl. Phys*., 86(7), 3983 - 3987.

De Heer, W. A.; Chatelain, A. & Ugarte, D. (1995). A carbon nanotube field-emission electron source. *Science,* 270, 1179 - 1180.

Deng, Z.; Yenilmez, E.; Leu, J.; Hoffman, J. E.; Straver, E. W. J.; Dai, H. & Moler, K. A. (2004). Metal-coated carbon nanotube tips for magnetic force microscopy. *Appl. Phys. Lett*., 85, 6263 – 6265.

Ebels, U.; Radulescu, A.; Henry, Y.; Piraux, L. & Ounadjela, K. (2000). Spin accumulation and domain wall magnetoresistance in 35 nm Co wires. *Phys. Rev. Lett.,* 84, 983-986.

Evans, P. R.; Yi G. & Schwarzacher W. (2000). Current perpendicular to plane giant magnetoresistance of multilayered nanowires electrodeposited in anodic aluminum oxide membranes. *Appl. Phys. Lett.,* 76, 481 – 483.

Evans, P. R.; Kullock, R.; Hendren, W. R.; Atkionson, R.; Pollard, R. J. & Eng, L. M. (2008). Optical transmission properties and electric field distribution of interacting 2D silver nanorod arrays. *Adv. Func. Mater.,* 18, 1075 – 1079.

Favier, F.; Walter, E.C.; Zach, M. P.; Benter, T. & Penner, R.M. (2001). Hydrogen sensors and switches from electrodeposited palladium mesowire arrays. *Science*, 293, 2227-2231.

Fleischmann, M.; Hendra, P.J. & McQuillan, A.J. (1974). Raman spectra of pyridine adsorbed at a silver electrode. *Chem. Phys. Lett*., 26(2), 163 – 166.

Fodor, P. S.; Tsoi, G. M. & Wenger, L. E. (2008). Investigation of magnetic interactions in large arrays of magnetic nanowires. *J. Appl. Phys.,* 103, 07B713-3.

Foong, T. R. B.; Sellinger, A. & Xu, X. (2008). Origin of the bottlenecks in preparing anodized aluminium oxide (AAO) templates on ITO glass. *ACS Nano*, 2(11), 2250 – 2256.

Fournier-Bidoz, S.; Kitaev, V.; Routkevich, D.; Manners, I. & Ozin, G.A. (2004). Highly ordered nanosphere imprinted nanochannel alumina (NINA). *Adv. Mater*., 16, 2193-2196.

Furneaux, R. C.; Rigby, W. R. & Davidson, A. P. (1989). The formation of controlled-porosity membranes from anodically oxidized aluminium. *Nature,* 337, 147 - 149.

Garcia-Martin, J. M.; Thiaville, A.; Miltat, J.; Okuna, T.; Vila, L. & Piraux, L. (2004). Imaging magnetic vortices by magnetic force microscopy: experiments and modelling. *J. Phys. D: Appl. Phys*., 37, 965 – 972.

García-Vidal, F. J. & Pendry, J. B. (1996). Collective Theory for Surface Enhanced Raman Scattering. *Phys. Rev. Lett.*, 77, 1163 – 1166.

Genov, D.A.; Sarychev, A.K.; Shalaev, M. & Wei, A. (2004). Resonant field enhancements from metal nanoparticle arrays. *Nano Lett.*, 4(1), 153 – 158.

Gingery, D. & Buhlmann, P. (2007). Single-step electrochemical method for producing very sharp Au scanning tunneling microscopy tips. *Rev. Sci. Instrum*., 78, 113703 - 113.

Gochowski E. (2003). The HDD roadmap. Published online by Hitachi Global Storage Technologies, Inc., http://colossalstorage.net/hdd_technology2003.pdf.

Grimsditch, M.; Jaccard, Y. & Ivan Schuller, K. (1998). Magnetic anisotropies in dot arrays: Shape anisotropy versus coupling. *Phys. Rev*. B, 58, 11539-11543.

Hafner, J. H.; Cheung, C.-L.; Oosterkamp, T. H. & Lieber, C. M. (2001). High-yield assembly of individual single-walled carbon nanotube tips for scanning probe microscopies. *J. Phys. Chem. B*, 105 (4), 743 – 746.

Huang, X.; Tan, L.; Cho, H. & Stadler, B. J. H. (2009). Magnetoresistance and spin transfer torque in electrodeposited Co/Cu multilayered nanowire arrays with small diameters. *J. Appl. Phys*., 105, 07D128-3.

Hurst, S. J.; Payne, E. K.; Qin, L. & Mirkin, C. A. (2006). Multisegmented one-dimensional nanorods prepared by hard-template synthetic methods. *Angew. Chem. Int. Ed*., 45, 2672 – 2692.

Jessensky, O.; Müller, F. & Gösele, U. (1998). Self-organized formation of hexagonal pore structures in anodic alumina. *J. Electrochem. Soc*., 145, 3735 – 3740.

Kabashin, A.V.; Evans, P.; Pastkovsky, S.; Hendren, W.; Wurtz, G. A.; Atkinson, R.; Pollard, R.; Podolskiy, V.A. & Zayats, A. V. (2009). Plasmonic nanorod metamaterials for biosensing. *Nature Mater*., doi:10.1038/NMAT2546.

Kahl, M. & Voges, E. (2000). Analysis of plasmon resonance and surface-enhanced Raman scattering on periodic silver structures. *Phys. Rev. B,* 61(20), 14078 – 14088.

Kaitsu, I.; Inamura, R.; Toda, J. & Morita, T. (2006). Ultra high density perpendicular magnetic recording technologies. *Fujitsu Sci. Tech. J.,* 42(1), 122 – 130.

Kartopu, G.; Es-Souni, M.; Sapelkin, A.V. & Dunstan, D. (2006). A novel SERS-active substrate system: Template-grown nanodot-film structures. *Phys. stat. sol.* (a), 203(10), R82 – R84.

Kartopu, G.; Yalçin, O.; Es-Souni, M. & Başaran, A. C. (2008a). Magnetization behavior of ordered and high density Co nanowire arrays with varying aspect ratio. *J. Appl. Phys*., 103, 093915-6.

Kartopu, G.; Es-Souni, M.; Sapelkin, A.V. & Dunstan, D. (2008b). Large-scale, reliable, and robust SERS-active nanowire-substrates prepared using porous alumina templates. *J. Nanosci. Nanotech*., 8(2), 931 – 935.

Kartopu, G.; Habouti, S. & Es-Souni, M. E. (2008c). Synthesis of palladium nanowire arrays with controlled length and diameter. *Mat. Chem. Phys*., 107, 226 – 230.

Keller, F.; Hunter, M. S. & Robinson, D. L. (1953). Structural features of oxide coatings on aluminium. *J. Electrochem. Soc*., 100 (9), 411-419.

Kim, B.; Park, S.; McCarthy, T.J. & Russell, T.P. (2007). Fabrication of ordered anodic aluminum oxide using a solvent-induced array of block-copolymer micelles. *Small*, 3(11), 1869-1872.

Kim, C.; Gu, W.; Briceno, M.; Robertson, I. M.; Choi, H. & Kim, K. (2008). Adv. Mater., Copper nanowires with a five-twinned structure grown by chemical vapor deposition. *Adv. Mater.*, 20(10), 1859 – 1863.

Kim, D.; Bourée, J.-E. & Kim, S. Y. (2009). Calculation of the field enhancement for a nanotube array and its emission properties. *J. Appl. Phys*., 105, 084315-5.

Kim, K. T.; Sim, S. J. & Cho, S. M. (2006). Hydrogen gas sensor using Pd nanowires electrodeposited into anodized alumina template. *IEEE Sens. J.,* 6(3), 509 – 513.

Kline, T. R.; Tian, M.; Wang, J.; Sen, A.; Chan, M. W. H. & Mallouk, T. E. (2006). Templategrown metal nanowires. *Inorg. Chem*., 45, 7555 – 7565.

Kolmakov, A.; Zhang, Y.; Cheng, G. & Moskovits, M. (2003). Detection of CO and O_2 using tin oxide nanowire sensors. *Adv. Mater.,* 15(12), 997 – 1000.

Krishnan, R. & Thompson, C.V. (2007). Monodomain high-aspect-ratio 2D and 3D ordered porous alumina structures with independently controlled pore spacing and diameter. *Adv. Mater*., 19, 988-992.

Kumar, A.; Fähler, S.; Schlörb, H.; Leistner, K. & Schultz L. (2006). Competition between shape anisotropy and magnetoelastic anisotropy in Ni nanowires electrodeposited within alumina templates. *Phys. Rev*. B, 73, 064421-064425.

Lee, J. H.; Wu, J. H.; Liu, H. L.; Cho, J. U.; Cho, M. K.; An, B. H.; Min, J. H.; Noh, S. J. & Kim, Y. K. (2007). Iron-gold barcode nanowires. *Angew. Chem. Int. Ed*., 46, 3663 – 3667.

Lee, W.; Ji, R.; Gösele, U. & Nielsch, K. (2006). Fast fabrication of long-range ordered porous alumina membranes by hard anodization. *Nature Mater*., 5, 741 – 747.

Li, A. P.; Müller, F.; Birner, A.; Nielsch, K. & Gösele, U. (1998). Hexagonal pore arrays with a 50–420 nm interpore distance formed by self-organization in anodic alumina. *J. Appl. Phys*., 84, 6023 – 6026.

Liang, J.; Chik, H. & Xu, J. (2002). Nonlithographic fabrication of lateral superlattices for nanometric electromagnetic-optic applications. *IEEE J. Quantum Electron*., 8(5), 998 – 1008.

Liu, N.W.; Datta, A; Liu, C.Y. & Wang, Y.L. (2003). High-speed focused-ion-beam patterning for guiding the growth of anodic alumina nanochannel arrays. *Appl. Phys. Lett*., 82, 1281-1283.

Luo, S. H.; Wan, Q.; Liu, W. L.; Zhang, M.; Di, Z. F.; Wang, S. Y.; Song, Z. T.; Lin, C. L. & Dai, J. Y. (2004). Vacuum electron field emission from SnO_2 nanowhiskers synthesized by thermal evaporation. *Nanotechnology*, 15, 1424 – 1427.

Mallet, J.; Yu-Zhang, K.; Mátéfi-Tempfli, S.; Mátéfi-Tempfli, M. & Piraux, L. (2005). Electrodeposited $L1_0$ Co_xPt_{1-x} nanowires. *J. Phys. D: Appl. Phys*, 38, 909 – 914.

Martin, C. R. (1994). Nanomaterials: A membrane-based synthetic approach. *Science*, 266, 1961 - 1966.

Martin, C. R. & Baker, L. A. (2005). Expanding the molecular electronics toolbox. *Science*, 309, 67 – 68.

Masuda, H. & Fukuda, K. (1995). Ordered metal nanohole arrays made by a two-step replication of honeycomb structures of anodic alumina. *Science*, 268, 1466 – 1468.

Masuda, H.; Yamada, H; Satoh, M.; Asoh, H.; Nakao, M. & Tamamura, T. (1997). Highly ordered nanochannel-array architecture in anodic alumina. *Appl. Phys. Lett*., 71, 2770-2772.

Mátéfi-Tempfli, S.; Mátéfi-Tempfli, M. & Piraux, L. (2009). Fabrication of nanowires and nanostructures: combining template synthesis with patterning methods. *App. Phys. A*, 96, 603 – 608.

Menon, L. ; Lu, W. T. ; Friedman, A. L. ; Bennett, S. P. ; Heiman, D. & Sridhar, S. (2008). Negative index metamaterials based on metal-dielectric nanocomposites for imaging applications. *J. Appl. Phys*., 93, 123117-3.

Metzger, R. M.; Konovalov, V. V.; Sun, M.; Xu, T.; Zangari, G.; Xu, B.; Benakli, M. & Doyle, W. D. (2000). Magnetic nanowires in hexagonally ordered pores of alumina. *IEEE Trans. Magn.*, 36(1), 30 – 35.

Mikulskas, I.; Juodkazis, S.; Tomašiūnas, R. & Dumas, J. G. (2001). Aluminum oxide phtonic crystals grown by a new hybrid method. *Adv. Mater.,* 13(20), 1574 – 1577.

Mock, J. J.; Oldenburg, S. J.; Smith, D. R.; Schultz, D. A. & Schultz, S. (2002). Composite plasmon resonant nanowires. *Nano Lett.*, 2(5), 465 – 469.

Murray, B. J.; Walter, E. C. & Penner, R. M. (2004). Amine vapor sensing with silver mesowires. *Nano Lett.,* 4(4), 665 – 670.

Nanosensors, (2008). www.nanosensors.com/Carbon_Nanotube_Probes.pdf

Nicewarner- Peña , S. R.; Freeman, R. G.; Reiss, B. D.; He, L.; Pena, D. J.; Walton, I. D.; Cromer, R.; Keating, C. D.; & Natan, M. J. (2001). Submicrometer metallic barcodes. *Science,* 294, 137 – 141.

Nie, S. & Emory, S.R. (1997). Probing single molecules and single nanoparticles by surfaceenhanced Raman scattering. *Science*, 275, 1102 - 1106.

Nielsch, K.; Müller, F.; Li, A. P. & Gösele, U. (2000). Uniform nickel deposition into ordered alumina pores by pulsed electrodeposition. *Adv. Mater*., 12(8), 582 – 586.

Nielsch, K.; Choi, J.; Schwirn, K. & Wehrspohn, R. B. & Gösele, U. (2002). Self-ordering regimes of porous alumina: The 10 porosity rule. *Nano Lett*., 2 (7), 677 – 680.

Nishio, K.; Yanagishita, T.; Hatakeyama, S.; Maegawa, H. & Masuda H. (2008). Fabrication of ideally ordered anodic porous alumina with large area by vacuum deposition of Al onto mold. *J. Vac. Sci. Technol. B*, 26(1), L10-L12.

Ohgai, T.; Hoffer, X.; Gravier, L.; Wegrowe, J.-E. & Ansermet J.-P. (2003). Bridging the gap between template synthesis and microelectronics: spin-valves and multilayers in self organized anodized alumimium nanopores. *Nanotechnology*, 14, 978 – 982.

O'Sullivan, J.P. & Wood, G.C. (1970). The morphology and mechanism of formation of porous anodic films on aluminium. *Proc. Roy. Soc. Lond*., 200, 5071-5076.

Peng, C.Y.; Liu, C.Y; Liu, N.W.; Wang, H.H.; Datta, A. & Wang, Y.L (2005). Ideally ordered 10 nm channel arrays grown by anodization of focused-ion-beam patterned aluminum. *J. Vac. Sci. Technol. B*, 23(2), 559-562.

Piraux, L.; George, J. M.; Despres, J. F.; Leroy, C.; Ferain, E.; Legras, R.; Ounadjela, K. & Fert, A. (1994). Giant magnetoresistance in magnetic multilayered nanowires. *Appl. Phys. Lett.*, 65(19), 2484 – 2446.

Piraux, L.; Dubois, S.; Fert, A. & Belliard, L. (1998). The temperature dependence of the perpendicular giant magnetoresistance in Co/Cu multilayered nanowires. *Eur. Phys. J. B*, 4(4), 413 – 420.

Pratt, W. P.; Lee, S.-F.; Slaughter, J. M.; Loloee, R.; Schroeder, P. A. & Bass, J. (1991). Perpendicular giant magnetoresistances of Ag/Co multilayers. *Phys. Rev. Lett*., 66, 3060 – 3063.

Qin, L.; Park, S.; Huang, L. & Mirkin, C. A. (2005). On-wire lithography. *Science*, 309, 113 – 115.

Qin, L.; Zou, S.; Xue, C.; Atkinson, A.; Schatz, G. C. & Mirkin, C. A. (2006). Designing, fabricating, and imaging Raman hot spots. *Proc. Nat. Acad. Sci.,* 103 (36), 13300 – 13303.

Quy, N. V.; Hoa, N. D; Yu, W. J.; Cho, Y. S.; Choi, G. S. & Kim, D. (2006). The use of anodic aluminium oxide templates for triode-type carbon nanotube field emission structures toward mass-production technology. *Nanotechnology,* 17, 2156 – 2160.

Renishaw plc, (2009). AFM-Raman system. http://www.renishaw.com/en/6638.aspx

Richter, H. J. (2007). The transition from longitudinal to perpendicular recording. *J. Phys. D: Appl. Phys.,* 40, R149 – R177.

Rivas, J.; Kazadi Mukenga Bantu, A.; Zaragoza, G.; Blanco, M. C. & López-Quintela, M. A. (2002). Preparation and magnetic behavior of arrays of electrodeposited Co nanowires. *J. Magn. Magn. Mater*., 249(1-2), 220-227.

Robinson, A. P.; Burnell, G.; Hu, M. & MacManus-Driscoll, J. L. (2007). Controlled, perfect ordering in ultrathin anodic aluminum oxide templates on silicon. *Appl. Phys. Lett*., 91, 143123-143125.

Sauer, M. G.; Brehm, G.; Schneider, S.; Graener, H.; Seifert, G.; Nielsch, K.; Choi, J.; Göring, P.; Gösele, U.; Miclea, P. & Wehrspohn, R.B. (2005). In situ surface-enhanced Raman spectroscopy of monodisperse silver nanowire arrays. *J. Appl. Phys*., 97, 024308-6.

Schönenberger, C.; van der Zande, B. M. I.; Fokkink, L. G. J.; Henny, M.; Schmid, C.; Krüger, M.; Bachtold, A.; Huber, R.; Birk, H. & Staufer, U. (1997). Template synthesis of nanowires in porous polycarbonate membranes: Electrochemistry and morphology. *J. Phys. Chem*. B, 101, 5497–5505.

Sommerlatte, J.; Nielsch, K. & Bötter, H. (2007). (In German) Thermoelektrische multitalente. *Physik Journal*, 6(5), 35 – 41.

Strijkers, G. J.; Dalderop, J. H. J.; Broeksteeg, M. A. A.; Swagten, H. J. M. & de Jonge, W. J. M. (1999). Structure and magnetization of arrays of electrodeposited Co wires in anodic alumina. *J. Appl. Phys*., 86, 5141-5145.

Sun, Z. & Kim, H.K. (2002). Growth of ordered, single-domain, alumina nanopore arrays with holographically patterned aluminium films. *Appl. Phys. Lett*., 81, 3458-3460.

Sysoev, V. V.; Button, B. K.; Wepsiec, K.; Dmitriev, S. & Kolmakov, A. (2006). Toward the nanoscopic "electronic nose": Hydrogen vs carbon monoxide discrimination with an array of individual metal oxide nano- and mesowire sensors. *Nano Lett.* 6(8), 1584 - 1588.

Tan, L.; McGary, P. & Stadler, B. J. H. (2008). Controlling the angular response of magnetoresistance in Co/Cu multilayered nanowires using Co crystallographic orientation. *J. Appl. Phys*., 103, 07D503-3.

Tang, X.-T.; Wang, G.-C. & Shima, M. (2007). Layer thickness dependence of CPP giant magnetoresistance in individual CoNi/Cu multilayer nanowires grown by electrodeposition. *Phys. Rev. B*, 75, 134404 – 134413.

The Nobel Foundation, http://nobelprize.org/nobel_prizes/physics/laureates/2007/.

Tresback, J. S.; Vasiliev, A. L. & Padture, N. P. (2005). Engineered metal-oxide-metal heterojunction nanowires. *J. Mater. Res*., 20(10), 2613 – 2617.

Tresback, J. S. & Padture, N. P. (2008).Low-temperature gas sensing in individual metal–oxide–metal heterojunction nanowires. *J. Mater. Res*., 23(8), 2047 – 2052.

Valet, T. & Fert, A. (1993). Theory of the perpendicular magnetoresistance in magnetic multilayers. *Phys. Rev*. B, 48, 7099 – 7113.

Vila, L.; Vincent, P.; Pra, L. D.-D.; Pirio, G.; Minoux, E.; Gangloff, L.; Demoustier-Champagne, S.; Sarazin, N.; Ferain, E.; Legras, R.; Piraux, L. & Legagneux, P. (2004). Growth and field-emission properties of vertically aligned cobalt nanowire arrays. *Nano Lett*., 4(3), 521 – 524.

Wade, T.L. & Wegrowe, J. E. (2005). Template synthesis of nanomaterials. *Eur. Phys. J. Appl. Phys*., 29(1), 3 – 22.

Wang, H.-H.; Liu, C.-Y.; Wu, S.B.; Liu, N.-W.; Peng, C.-Y.; Chan, T.-H.; Hsu, C.-F.; Wang, J.-K. & Wang, Y.-L. (2006). Highly Raman-enhancing substrates based on silver nanoparticle arrays with tunable sub-10 nm gaps. *Adv. Mater*., 18, 491 – 495.

Whitney, T. M.; Searson, P. C.; Jiang, J. S. & Chien, C. L. (1993). Fabrication and magnetic properties of arrays of metallic nanowires. *Scienc*e, 261, 1316 - 1319.

Wilson, N. R. & Macpherson, J. V. (2009). Carbon nanotube tips for atomic force microscopy. *Nature Nanotech*., 4, 483 – 491.

Yao, J.; Liu, Z.; Liu, Y.; Wang, Y.; Sun, C.; Bartal, G.; Stacy, A. M. & Zhang, X. (2008). Optical negative refraction in bulk metamaterials of nanowires. *Science*, 321, 930.

Yenilmez, E.; Wang, Q.; Chen, R. J.; Wang, D. & Dai, H. (2002). Wafer scale production of carbon nanotube scanning probe tips for atomic force microscopy. *Appl. Phys. Lett.,* 80, 2225 – 2227.

Yin, A. J.; Li, J.; Jian, W.; Bennett, A. J. & Xu, J. M. (2001). Fabrication of highly ordered metallic nanowire arrays by electrodeposition. *Appl. Phys. Lett.,* 79, 1039 – 1041.

Electrodeposited Nanowires and their Applications

Edited by Nicoleta Lupu

ISBN 978-953-7619-88-6
Hard cover, 228 pages
Publisher InTech
Published online 01, February, 2010
Published in print edition February, 2010

The book offers a new and complex perspective on the fabrication and use of electrodeposited nanowires for the design of efficient and competitive applications. While not pretending to be comprehensive, the book is addressing not only to researchers specialized in this field, but also to Ph.D. students, postdocs and experienced technical professionals.

How to reference

In order to correctly reference this scholarly work, feel free to copy and paste the following:

Giray Kartopu and Orhan Yalçın (2010). Fabrication and Applications of Metal Nanowire Arrays Electrodeposited in Ordered Porous Templates, Electrodeposited Nanowires and their Applications, Nicoleta Lupu (Ed.), ISBN: 978-953-7619-88-6, InTech, Available from: http://www.intechopen.com/books/electrodeposited-nanowires-and-their-applications/fabrication-and-applications-of-metal-nanowire-arrays-electrodeposited-in-ordered-porous-templates

INTECH
open science | open minds

InTech Europe
University Campus STeP Ri
Slavka Krautzeka 83/A
51000 Rijeka, Croatia
Phone: +385 (51) 770 447
Fax: +385 (51) 686 166
www.intechopen.com

InTech China
Unit 405, Office Block, Hotel Equatorial Shanghai
No.65, Yan An Road (West), Shanghai, 200040, China
中国上海市延安西路65号上海国际贵都大饭店办公楼405单元
Phone: +86-21-62489820
Fax: +86-21-62489821

IntechOpen